

GEOLOGY FOR SOCIETY

SINCE 1858



**GEOLOGICAL
SURVEY OF
NORWAY**

· NGU ·

NGU REPORT 2022.003

Testing the performance of Fuzzy C-means data clustering approach in the detection of weak zones in bedrock for the case of Knappe tunnel (ForForUT project)



Report no.: 2022.003	ISSN: 0800-3416 (print) ISSN: 2387-3515 (online)	Grading: Open	
Title: Testing the performance of Fuzzy C-means data clustering approach in the detection of weak zones in bedrock for the case of Knappe tunnel (ForForUT project)			
Authors: Georgios Tassis, Ying Wang, Jan Steinar Rønning		Client: Statens Vegvesen Vegdirektoratet / NGU	
County: Vestland		Commune: Bergen	
Map-sheet name (M=1:250.000): BERGEN		Map-sheet no. & name (M1:50.000): 1115 I Bergen	
Deposit name and grid-reference: Ringveg vest, Bergen 32V 293730 - 6696910		Number of pages: 44	Price (NOK): 168
Fieldwork carried out: 2009		Date of report: 5.7.2023	Project no.: 329500
		Person responsible:	
<p>Summary</p> <p>Near-surface geophysical applications employing multiple 2D methods that are mapping multiple properties along co-located profiles, enable new possibilities in exploring subsurface structures. Diverse data sets can now be cooperatively interpreted with the use of cluster analysis which is an unsupervised machine learning method that helps to explore patterns in data and separate them into groups based on similarity. In this report, we present our first attempt in testing this novel 2D method by applying cluster analysis on our previously published results from parts of the Knappe-tunnel.</p> <p>The now completed 3.8 km long Knappe tunnel west of the city of Bergen is a site where multimethod-based exploration is available but also a test area where resulting clustering interpretations can be directly compared to bedrock quality estimations carried out after its completion. In this framework, resistivity and P-wave velocity values for co-located profiles were automatically classified with the use of Fuzzy C-means clustering method. Two independent implementations of this method were utilized: one in-house ran by NGU-researcher Ying Wang, and another provided and ran by Dr Beatriz Benjumea of the Geological Survey of Spain. Hence, a large variety of 2D results were produced, enabling inherently joint interpretation of possible weak zones, in addition to those already extracted directly from the ERT and Refraction Seismic inversion results. Through this procedure we were able to test the performance of the Fuzzy C-means method independently and evaluate how systematic clustering results are, coming from two different algorithms.</p> <p>Our results indicate that we were not able to utilize cluster analysis in full in this first attempt due to limited knowledge concerning applicability of the method on vertical 2D geophysical profiling. However, new ideas and approaches were inspired that will be pursued in the future.</p>			
Keywords			
Geophysics	Cluster analysis	Fuzzy C-means method	
Refraction Seismic	Resistivity	Co-processing	
Weak zones in bedrock	Bedrock quality	Scientific report	

Table of contents

1. INTRODUCTION	5
2. METHOD	5
3. DATA DESCRIPTION & PREPARATION	6
4. METHODOLOGY	9
5. RESULTS	10
5.1 Profile P1_1	10
5.2 Profile P1_2	14
5.3 Profile P1_3	17
5.4 Profile P1_4-5	20
5.5 Profile P1_6-7	23
5.6 Profile P1_8	26
5.7 Profile P1_9	29
5.8 Profile P1_9.5	32
5.9 Profile P3	35
5.10 Profile P6	38
6. DISCUSSIONS & CONCLUSIONS	41
7. REFERENCES	43

1. INTRODUCTION

Over the last few years, NGU has repeatedly worked with reprocessing data from geophysical investigations performed at the site of Knappe tunnel, which is part of the ring road west of the city of Bergen (Rønning et al., 2016; Tassis et al., 2017; Tassis et al., 2018; Rønning et al., 2019). The variety of co-located ground geophysics at the site is one reason for doing so, but more importantly, it is the availability of detailed bedrock quality estimations done by geologists inside both tunnels that were built that constitute Knappe tunnel as a valuable test site. As follows, geophysical interpretations can be directly compared to geological observations and in this way safely evaluated and later improved. Reprocessing of both resistivity and refraction seismic profiling was therefore done in various stages during the last years, aimed at finetuning inversion procedures that could lead to better interpretations of possible weak zones in bedrock.

Conventionally, geoscientists with varying expertise and experience, process and interpret each type of geophysical data separately. Resistivity data were naturally processed, interpreted, and reported by NGU at the time when measurements were done (Ganerød et al., 2009) and so were the refraction seismic data by the private contractor who undertook the task (Wåle, 2009). Moreover, following the continuous development of new inversion software for both resistivity and refraction seismic data, all ground geophysics were reprocessed with special focus on refraction seismic inversion with the use of Rayfract software (Rohdewald, 2018). Our efforts were directed at refining our knowledge on the inversion procedure and eventually, our results proved that refraction seismic tomographic inversion can be utilized in detecting weak zones in bedrock alongside ERT (Rønning et al., 2016; Tassis et al., 2017; Tassis et al., 2018; Rønning et al., 2019; Rønning et al., 2020).

Naturally, the aforementioned standalone results are more than enough in providing the basis for interpretations about the subsurface geological conditions at Knappe tunnel and areas of low resistivity and P-wave velocity match the majority of bad bedrock quality observations. However, each of these two geophysical techniques maps a different physical property of the ground and therefore, no singular method could achieve a perfect score in detecting weak zones in bedrock. We therefore investigate the possibility of objectively integrating resistivity and P-wave velocity into clusters that might attain multigeophysical properties better associated with weak zones in bedrock than ERT and refraction seismic can individually achieve. In this report, we present the workflow and technical details of applying cluster analysis to previously reported results from Knappe tunnel, as part of the ForForUT project (Forbedrede Forundersøkelser for Utbygging Tunneler) which is a collaborative project with the Norwegian Public Roads Administration (Statens vegvesen, SVV).

2. METHOD

We apply the Fuzzy c-means (FCM) cluster analysis on co-located multi-geophysical data to generate cluster maps with integrated information which capture the spatial heterogeneity of the study region (2D depth sections in this case). The spatial heterogeneity gives indications about the geology variation. Cluster analysis is an unsupervised machine learning method that helps to explore patterns in the data and separate them into groups based on similarity. The chosen fuzzy c-means clustering algorithm (Bezdek et al. 1984) in our study has gained popularity and many successful

applications in geoscience (e.g.: Paasche *et al.* 2011; Song *et al.* 2017; Wang *et al.* 2021). The algorithm follows fuzzy logic principles (Novák *et al.* 1999), meaning each data point has a probability of belonging to each cluster, rather than completely belonging to just one specific cluster as it is the case in the traditional crisp *k*-means clustering algorithm. The probability of a data point belonging to a particular cluster is termed *membership* and ranges from 0 to 1. For each data point, its memberships to all clusters sum to 1.

It is important to note that various implementations of the FCM method exist, and researchers may have different preferences regarding their use and parameter tuning. As a result, different researchers may produce different results, even when using the same FCM method on the same dataset. In our study, the NGU in-house FCM analysis was conducted using the Python package Scikit-fuzzy, version 0.4.2, developed by Warner *et al.* (2019).

3. DATA DESCRIPTION & PREPARATION

Co-location of 2D profiles is a prerequisite for applying cluster analysis and **figures 1** and **2** show that this requirement is mostly met for the ground geophysics carried out at the Knappe tunnel site. However, this survey was not planned for the level of detailed joint interpretation clustering offers, therefore no special care was taken in the accurate matching between resistivity tomography and refraction seismic lines. Examining the map shown in **figures 1** and **2** in detail, small discrepancies in the positioning of the profiling for the two methods are easily detectable. In addition, weak zones mapped by geologists at the surface and plotted in the same map using light green dotted lines, display the acute angle at which the tunnel routes are intersected by the weak zone regime in the area. This geometrical specificity is expected to have an effect on the accuracy of our joint interpretation since our evaluations are based on the comparison between bedrock quality estimations in two separate tunnels and 2D profiles located in the interspace between them (tunnel separation ~20 meters). Such acute angles guarantee a displacement in the positioning of weak zones in bedrock inside the two tunnels and therefore, positions of poor and very poor bedrock quality shown in orange and red respectively in **figures 1** and **2**, cannot be safely compared to neither our geophysical, nor our clustering interpretations.

As mentioned above, we will be feeding the FCM cluster analysis method with data that are previously published in NGU report 2019.014 (Rønning *et al.*, 2019). No re-processing is required, just the fulfilment of the condition for co-location of inversion results. In this context, all inverted resistivities and P-wave velocities were re-gridded in order to occupy the same points in 2D space. By superimposing the matching ERT and refraction seismic profiles afterwards, we were able to isolate all co-located points, discarding at the same time all non-matching ones. Such points can occur due to differences in topography between non-perfectly matching 2D profiles, the inherent difference between the trapezoid depth coverage of ERT in relation to the more rounded ray coverage of refraction seismic and/or extrapolation out of the original coverage as a result of detailed re-gridding. Admittedly, having limited control over the positioning of ground geophysics does not facilitate data preparation for cluster analysis which undermines the result. However, this is an initial attempt at implementing the method and therefore some leniency is allowed.

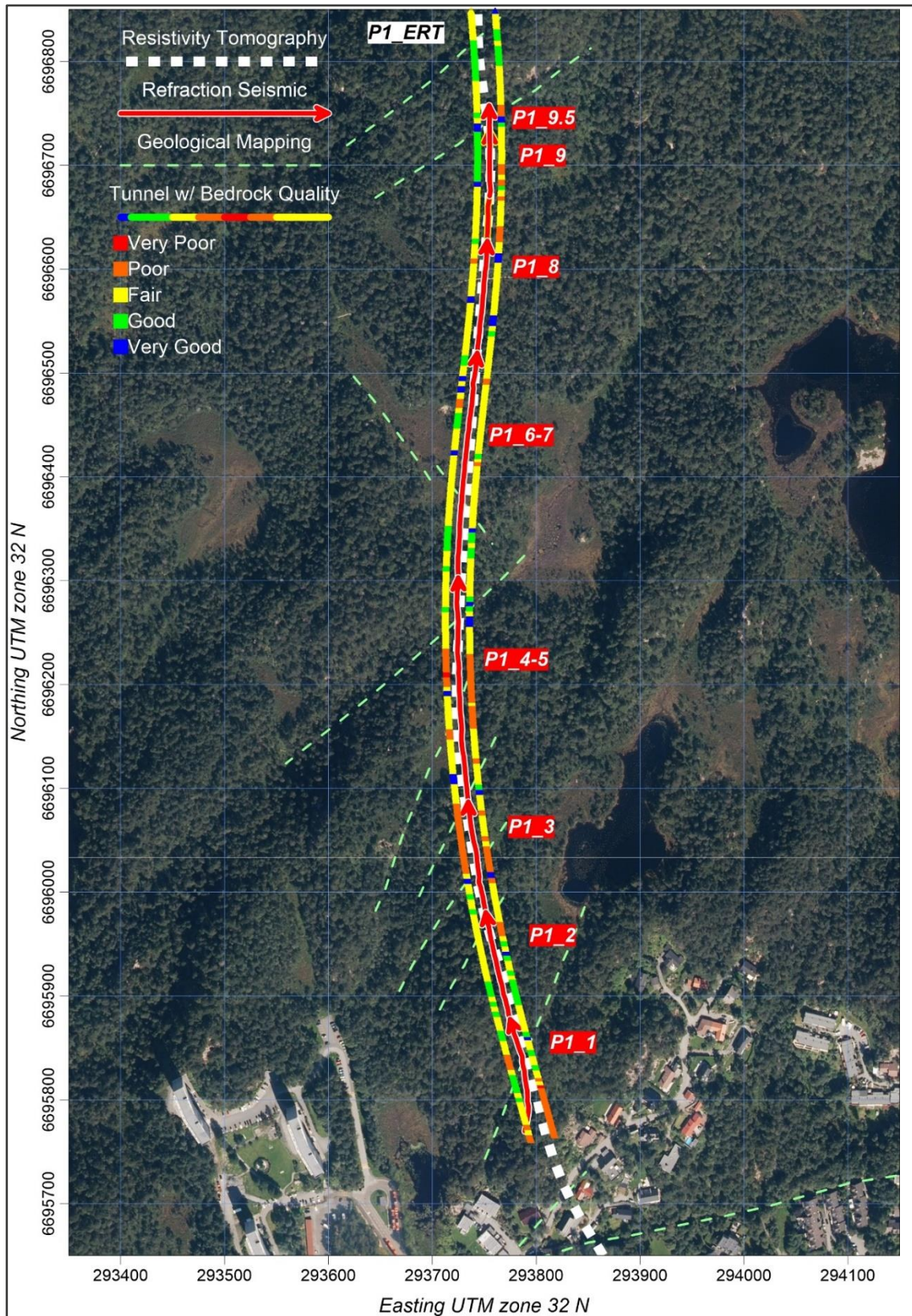


Figure 1: Positioning for the eight parts of profile 1 (P1) of the ground geophysics carried out at Knappe in relation to the bedrock quality estimations at the tunnel level and geological mapping performed at the surface (Norge I bilder, 2022).

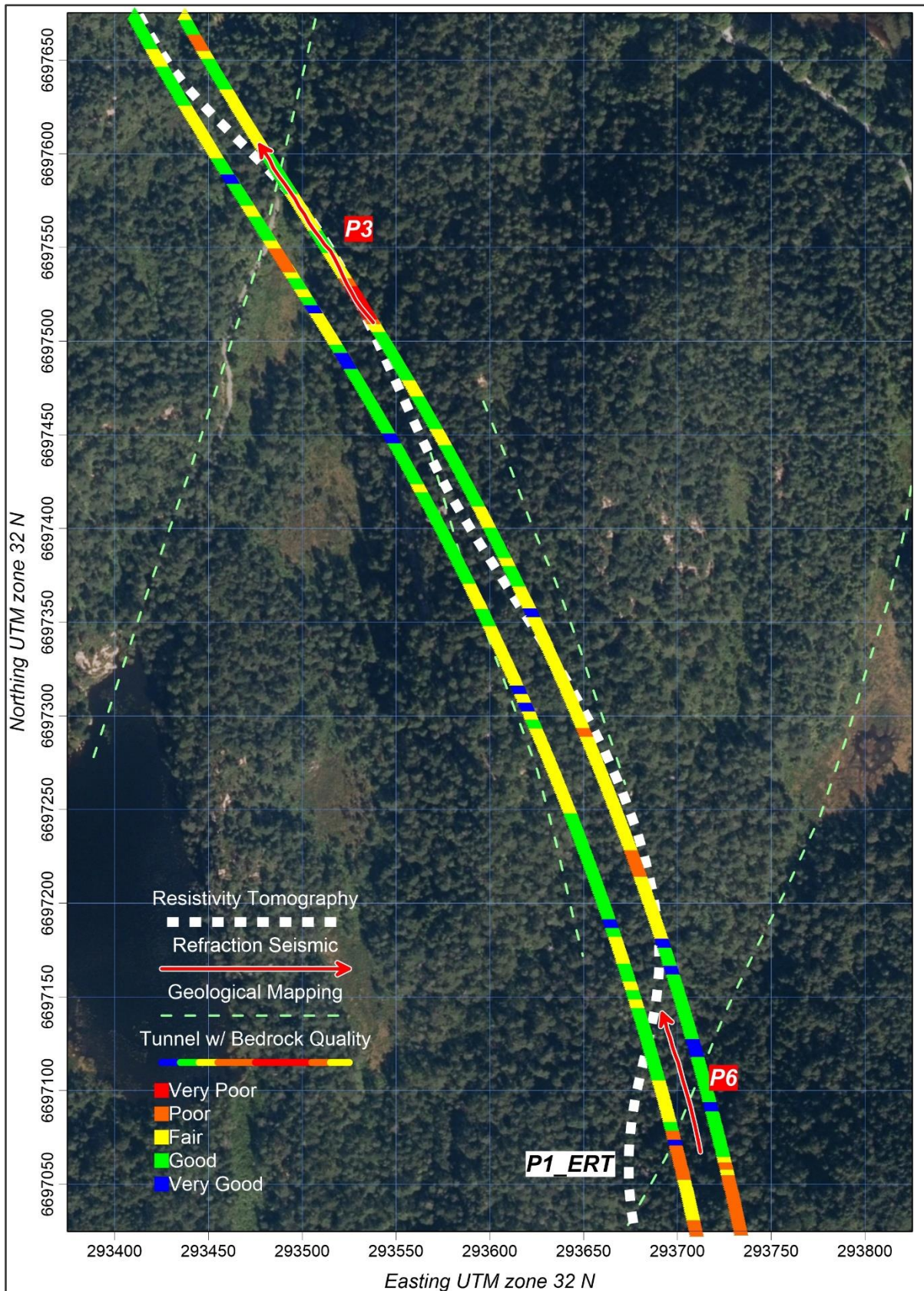


Figure 2: Positioning for profiles 3 and 6 (P3 – P6) of the ground geophysics carried out at Knappe in relation to the bedrock quality estimations at the tunnel level and geological mapping performed at the surface (Norge I bilder, 2022).

4. METHODOLOGY

In total, 10 pairs of profiles measured at the Knappe tunnel area – eight of which are shown in **figure 1** – will be examined in the context of cluster analysis by partitioning velocity with P-wave velocity in clusters.

The fuzzy C-means method requires the user to specify the number of clusters to be generated. Different mathematical criteria, such as the Silhouette score (Rousseeuw 1987), the Caliński-Harabasz score (Caliński & Harabasz 1974), and the Elbow method (Thorndike 1953), were consulted to evaluate the quality of clustering by assessing the separability between clusters and the similarity within each cluster. Wang et al. (2021) provides an explanation of how to use these criteria to determine the optimal cluster number for a given dataset. In this study, all three criteria were computed for a range of cluster numbers (from 2 to 20) on separate profiles, as well as on the entire dataset. Summarizing the results, we decided five to eight clusters should all be further tested in the aim to balance between the mathematical measures of clustering performance and the level of detail in the geological information that is accommodated by the clustering result. In this sense, we tested every case from five to eight clusters, which resulted in four different outcomes for every profile pair.

The workflow of the methodology in detail, is as follows:

- Both ERT and refraction seismic data were individually inverted with the use of relevant software i.e., RES2DINV (Loke, 2018) and Rayfract (Rohdewald, 2018) respectively.
- The resulting point resistivities and P-wave velocities were resampled in a common spatial grid since ERT was measured with 10-meter electrode spacing and refraction seismic with 5-meter geophone spacing.
- Parameter space was built where each cell is characterized by the two physical parameters mentioned above.
- FCM method was applied by grouping the data in the parameter space into five to eight clusters. Every sample was marked with partial membership to each cluster.
- The cluster value corresponding to the maximum membership was transformed from the parameter space back to the model domain.

It should be noted that for this first attempt at applying FCM clustering on resistivity versus P-wave velocity data, the whole procedure was kept simple and uncomplicated. We have utilized results that were obtained by inversions that did not take under consideration possible clustering efforts to follow, resistivities were fed to the algorithm in their absolute value and not their logarithm, and clustering was performed at a default level. It should also be noted that clustering between resistivity and velocity is not a new research topic, but the aim of surveys prior to ours was the differentiation between horizontal layering (Hellman et al., 2017; Benjumea et al., 2021) whereas our efforts are more focused on vertical structures. This raised level of complexity combined with our simplified clustering approach, lowers the expectations for acquiring robust results at this stage. However, we aspire that via this experiment, the basis for a more sophisticated approach will be set.

5. RESULTS

The outlay for presenting FCM cluster analysis results is as follows: for each of the ten profiles examined, two sets of clustering results will be shown based on the algorithm used i.e., external and internal to NGU. Within each 2D profile plot, bedrock quality estimations are also included by plotting the eastern section's estimations at the ceiling and the western section's estimations at the floor of the tunnel respectively. This way, all available information on both tunnels is included in each illustration along with a representation of the tunnelling dimensions in relation to the coverage of the geophysics.

Next to each profile, the parameter space of the cluster analysis is presented i.e., a plot between velocity (x-axis) and resistivity (y-axis) which displays the space that each cluster occupies, and which values are paired within it. Our goal is to identify, if possible, clusters matching the tunnel segments marked with orange (poor) and red (very poor) colours. However, the geometry of the weakness zones in the area must also be considered when comparing poor and very poor bedrock quality localities to the clustering results. As seen in **figure 1**, the weakness zones identified at the surface cross the tunnels/geophysics mainly along the SW-NE direction at acute angles with the exception of a SE-NW zone which crosses profile P1_6-7. Therefore, a few meters forward offset for the western tunnel and a few meters backward offset for the eastern one should be expected when trying to match questionable quality bedrock to clusters. More complex geometries should also be considered based on differences in bedrock quality between the two neighbouring tunnels and possible tilting of the zones seen at the surface, followed through to the depth at which the tunnels were built.

Presenting clustering results between resistivity and P-wave velocity is challenging, particularly when it comes to choosing a suitable colour scale. Traditionally, a standard rainbow colour scale is used in geophysics where cold colours indicate low parameter values and warm colours, high. However, clustering does not necessarily match low resistivities to low velocities that are otherwise used for interpreting potential weak zones in ERT and Refraction Seismic surveys. Instead, clusters span over a wide range of values, creating brackets of these two physical properties that do not have a direct physical meaning. It was therefore particularly difficult to assign a colour to each resulting cluster in a robust way that resembles what a standard rainbow colour scale offers. Hence, we picked a scale with fewer colours, varying from purple to green and yellow. Our colouring strategy follows an outward concentric colouring pattern which is snaking among the different clusters while trying at the same time to maintain the main philosophy that purples and dark greens represent possible weak zones, while light greens and yellows represent good quality bedrock. Whether this is a feasible way for assigning colours to our results or not, will be dictated by the degree of correlation between the purple/dark green clusters in each profile and the segments of the tunnels evaluated as orange or red.

5.1 Profile P1_1

Figure 3 presents the clustering results using the external algorithm (Spanish) while **figure 4** shows the results obtained from the internal NGU algorithm. Estimations at depth indicate that Knappe tunnel is cutting through an area of generally poor bedrock quality, even though observations inside the two tunnels are quite inconsistent to each other. As seen in both figures, the coverage of profile P1_1 is not extensive enough to

reach the level of the tunnel therefore, the degree of correlation between clusters and bedrock quality estimations will be done by extrapolating interpretations downward.

Examining the parameter space plots we can easily deduce that for equal number of clusters applied, the two algorithms used in this study produce different cluster distributions. It is therefore evident that none of the resulting clusters can singlehandedly map poor bedrock quality. Hence, interpretations must be done intuitively i.e., in an intra-cluster mode that follows transition zones between clusters (colours) found in the lower left quadrant of the parameter space plot. Depending on the number of clusters employed, weak zones will be mapped following the higher cluster number serially i.e., the darker colours in each example.

Both versions of FCM clustering implementation are quite consistent in classifying bedrock regardless of cluster number. In both sets of results, the first half of profile P1_1 is characterized by light green/yellow clusters whereas the other half is dominated by darker green/purple hues. In accordance with the interpretation principle described above, it is indicated that bedrock quality is better on the first half of the profile and worse on the second half. However, the observations at the tunnel level show the exact opposite, with the largest extent of poor bedrock being found at the eastern leg of the tunnel, 40 meters below the geophysics coverage. Nevertheless, the majority of clustering results shows that bedrock quality is beginning to change beneath clusters one and two (yellow/light green) while immediate neighbouring clusters indicate inclining structures of lower resistivity and velocity. Such structures are marked with dotted lines and gridded areas, showing a possible interpretation that could match the tunnel observations in depth for the first half of P1_1.

Regarding the second half of the profile, clustering reveals a set of lateral variations which are typically coloured accordingly to the higher serial number of clusters and thus indicating questionable bedrock quality. In depth, there is a clear weak zone mapped in the west tunnel that matches a very prominent vertical structure in all clustering results. However, as the serial number for clusters increases, this structure appears to be divided in two by good bedrock quality (cluster two or three). For that reason, our interpretation marks to possible weak zones divided by good bedrock, one that tilts southwards and by widening in depth matches the poor bedrock area in the eastern tunnel, and a second one which continues downward and meet the prominent poor bedrock zone in the western tunnel. In addition, a third possible weak zone may be interpreted at the end of the profile but since it is tilting northwards, it is possibly associated with a weak zone farther down the route of the tunnel or even truncated in depth and not reaching the tunnel level at all.

For profile P1_1 we may note that more clusters are better than fewer, especially when the internal NGU algorithm is applied. Hence, seven seems to be the ideal cluster number for highlighting all information enclosed in our data. Fewer clusters simplify the acquired image but does not hurt interpretation for this case, except for the possible third zone at the end of the profile. Generally, results with more clusters are dominated by darker colours which agrees with the bedrock quality estimated within this stretch of the tunnel. Interpretations based on the clusters occupying the lower left quadrant of each parameter space plot remain relatively consistent regardless of algorithm and cluster number. Small differences in the geometry of the interpreted fracture zones are of course due to the intuitive nature of our approach and the unavoidable bias introduced by the knowledge of the weak zone positioning.

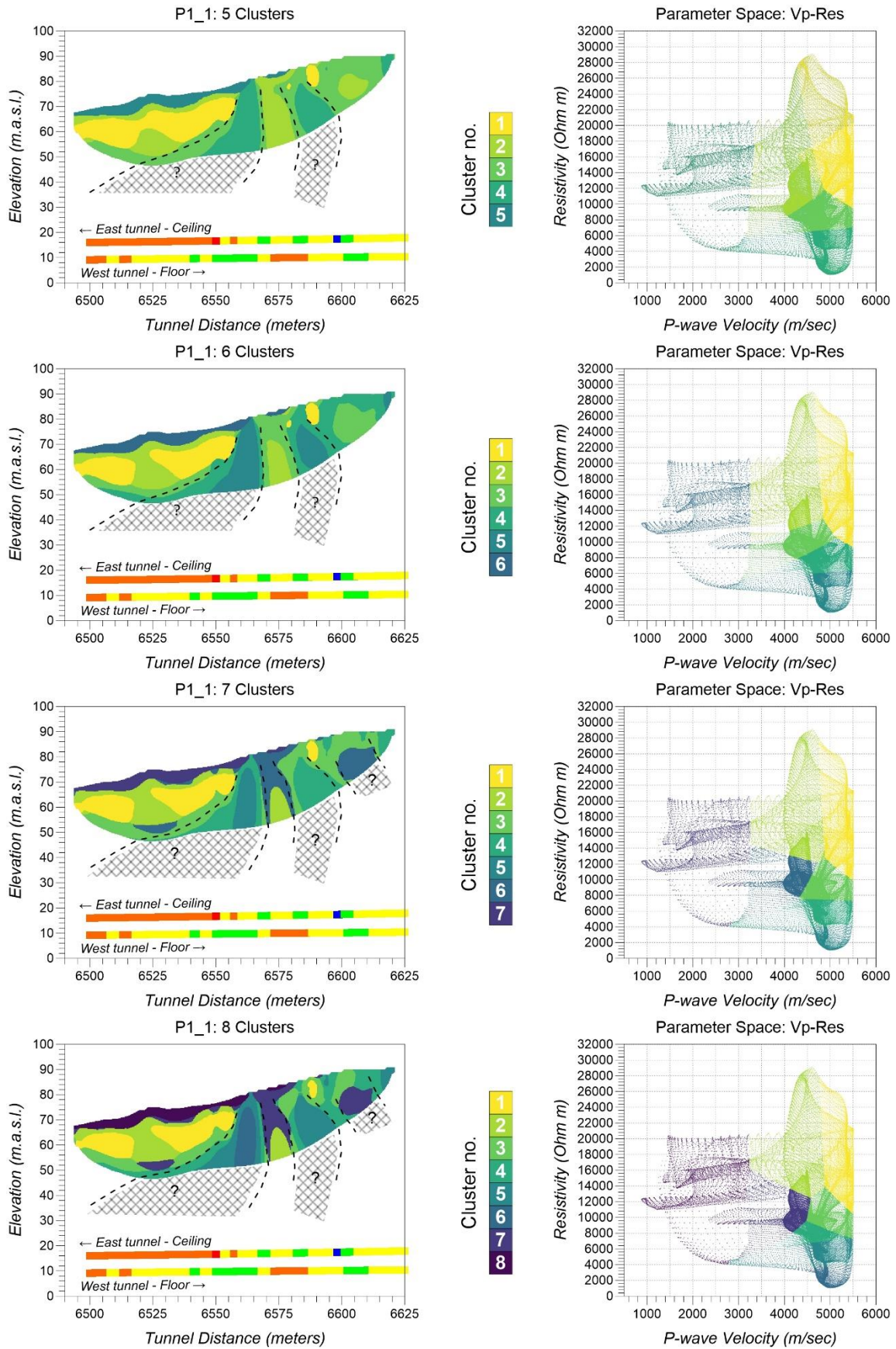


Figure 3: FCM cluster analysis results for Profile P1_1 using five, six, seven and eight clusters (left, top to bottom) and respective parameter space plots (right, top to bottom). Conducted by Dr B. Benjumea.

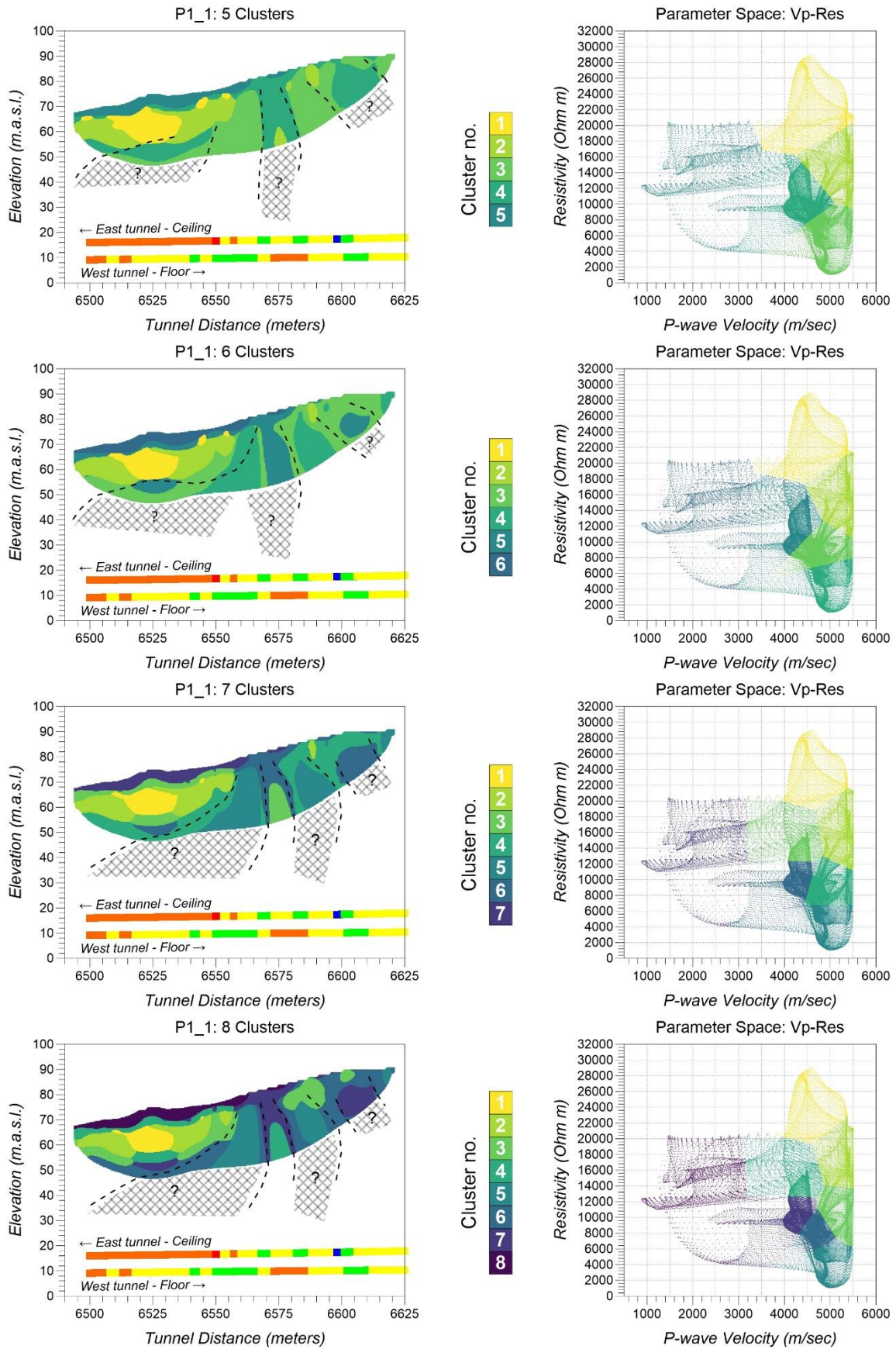


Figure 4: FCM cluster analysis results for Profile P1_1 using five, six, seven and eight clusters (left, top to bottom) and respective parameter space plots (right, top to bottom). Conducted by NGU researcher Ying Wang.

5.2 Profile P1_2

Clustering results for profile P1_2 conducted externally and in-house are shown in **figures 5** and **6** respectively. As in profile P1_1, the geophysical coverage does not reach the tunnel level and therefore interpretations have to be once more extrapolated downwards.

Regarding bedrock quality at the tunnel level, it appears to be at least fair or better throughout the length of the profile with the exception of a zone marked inside the eastern tunnel, but at the same time is not found in the western leg. Regardless of this small inconsistency, tunnelling appears to go through good quality bedrock, especially on the first half of the profile whereas a minor degradation can be observed in the second half.

All clustering results appear to be quite robust in depicting this gradual lateral change in bedrock quality seen in depth, with light colours dominating in the beginning and gradually becoming darker as we move along profile P1_2. This change is marked by a pronounced vertical structure which stands out due to the fact that it is consistently coloured accordingly to the highest cluster number (5 to 8). Moreover, it appears to be inclining towards the north and therefore matching the poor bedrock quality section mapped inside the eastern tunnel pretty well, about 30 meters below the maximum coverage of geophysics. The manifestation of this possible weak zone is present in all results and is marked with two dotted lines and a gridded rectangle.

We have seen that increasing the number of clusters also increases resolution in both clustering results and this is the case for profile P1_2 too. Especially for the case of seven and eight classifications, the use of more clusters reveals another possible weak zone a few meters after the aforementioned. It appears to be vertical and aiming almost directly at the poor bedrock quality stretch below it. This structure can be interpreted in seven out of eight results and only the application of 5 clusters on the external algorithm fails to delineate it (**figure 5** – top left plot). We may then assume that these two zones are merging in depth and become one of significantly smaller dimensions compared to their superficial extent.

The results of applying FCM clustering on profile P1_2 suggest once more that six or seven clusters produce the most meaningful and easily interpretable outcomes regardless of implementation employed. Good quality bedrock is always very well defined by the first clusters but interpretation on vertical structures with fewer clusters can be deceptive. In this case, using five clusters led to the masking of a possible vertical structure. On the other hand, choosing eight did not enhance resolution, even though no artificial effects were generated for this example.

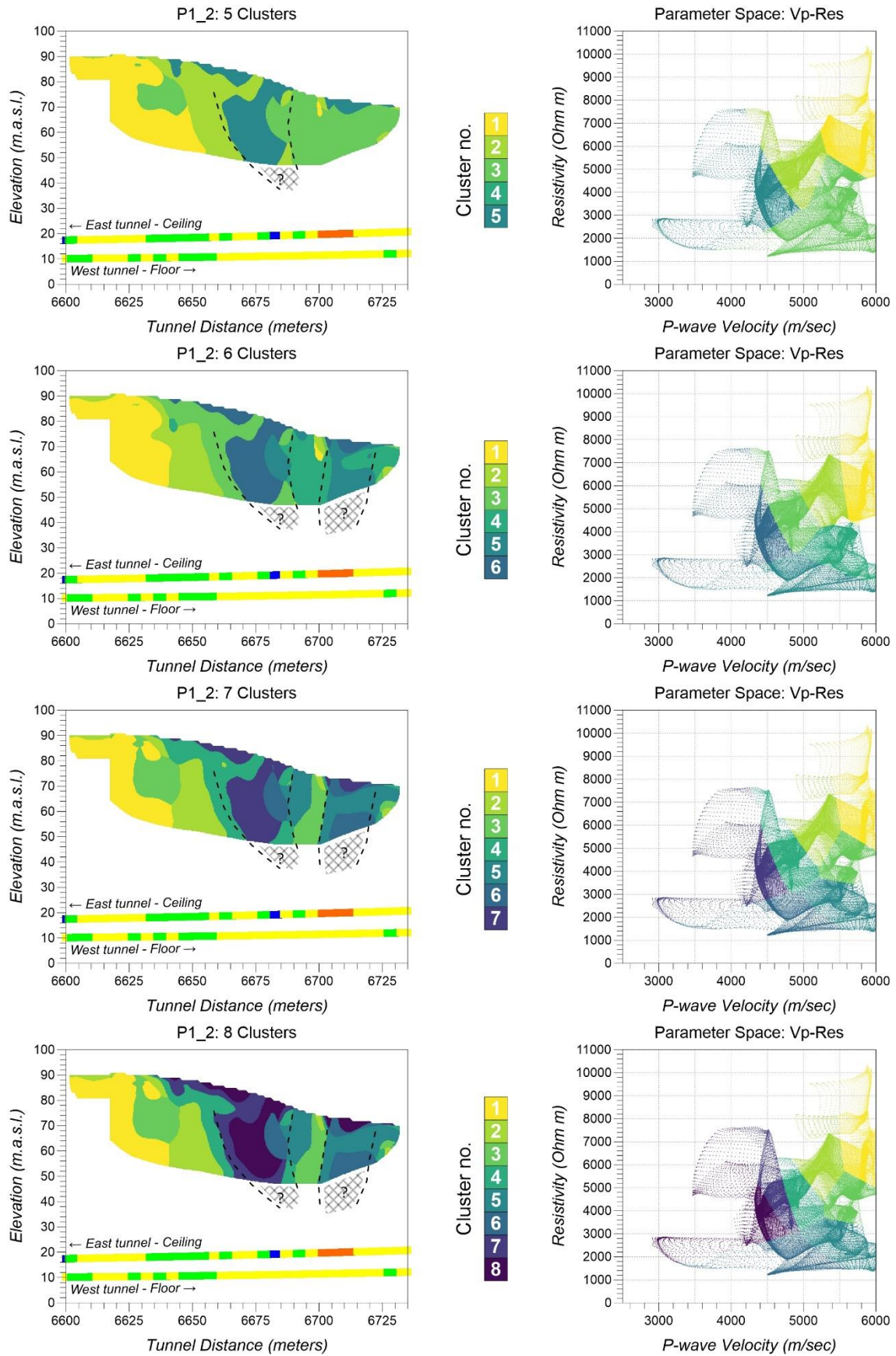


Figure 5: FCM cluster analysis results for Profile P1_2 using five, six, seven and eight clusters (left, top to bottom) and respective parameter space plots (right, top to bottom). Conducted by Dr B. Benjumea.

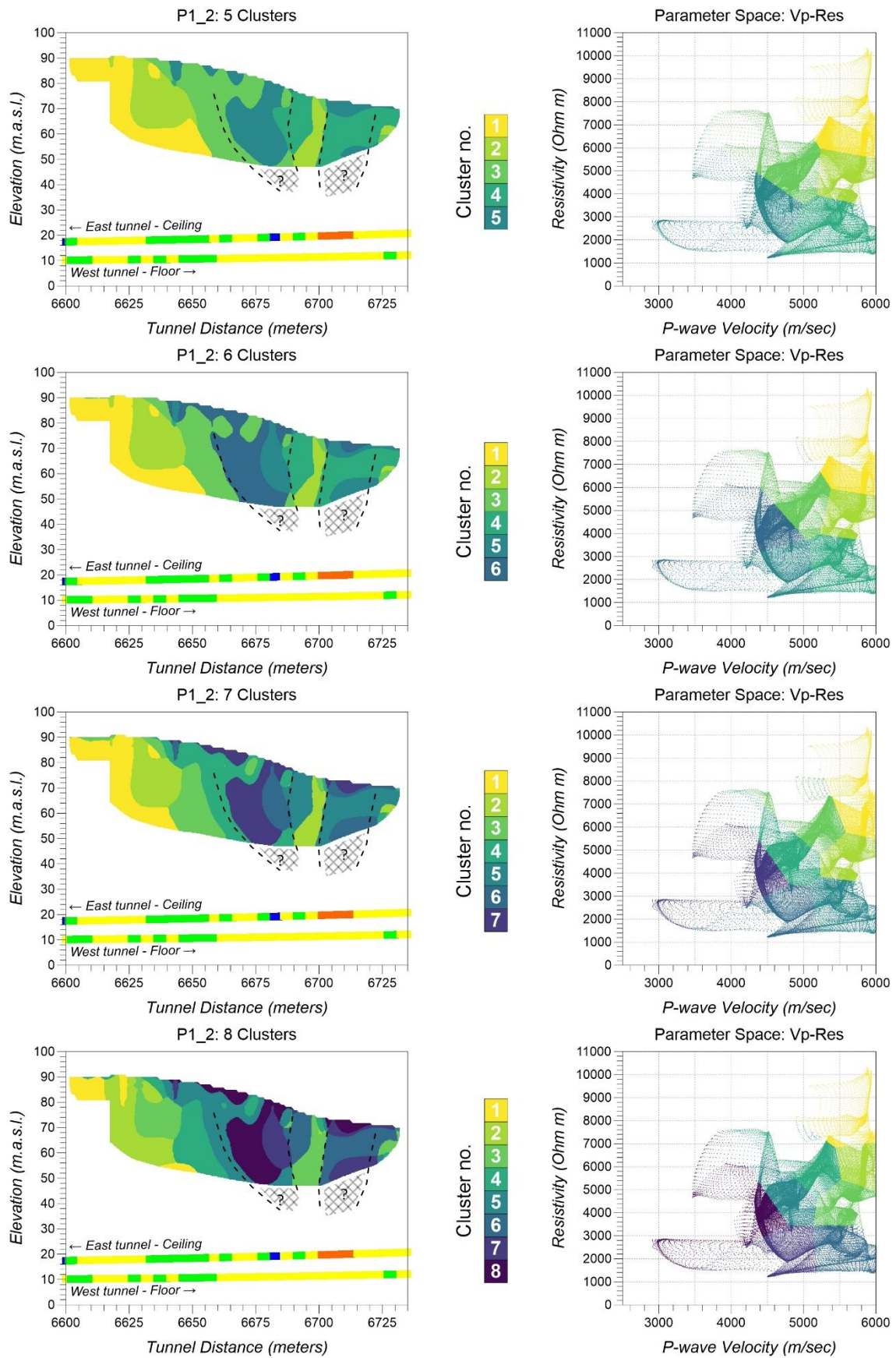


Figure 6: FCM cluster analysis results for Profile P1_2 using five, six, seven and eight clusters (left, top to bottom) and respective parameter space plots (right, top to bottom). Conducted by NGU researcher Ying Wang.

5.3 Profile P1_3

Figures 7 and **8** present the results of implementing the FCM clustering method on profile P1_3. **Figure 7** displays four classification examples produced with the use of external implementation while **figure 8** the respective results of the internal NGU implementation. The distance between the top of the tunnel and the deepest geophysical measurement is around 20 meters which is closer than the two profiles prior to P1_3. Still, extrapolating interpretations to the tunnel level depth is required.

Bedrock quality estimations along this stretch indicate long segments of poor quality in both tunnels with the most extensive areas being at the centre of the profile. Discrepancies are still observed in the conditions mapped in each channel with the western tunnel exhibiting a more continuous distribution of bad quality bedrock as opposed to the more disconnected outlook of the eastern tunnel. Overall, the middle and last part of the profile is the most interesting in relation to detecting possible weak zones.

Again, interpretations are based on the layout of the highest clustering numbers per case i.e., by identifying areas characterized by a combination of the darkest green / purple colours per colour scale utilized. Such an area is found in every result shown in **figures 7** and **8** occupying a broad area at the middle of profile P1_3. The geometric nuances of this area are changing with increasing the number of different clusters utilized, but the limits of this possible weak zone remain in good agreement with what was evaluated at the tunnel level, especially with the broad poor bedrock quality zone in the eastern tunnel. This respective zone in the western tunnel appears to be wider, so a change in width is expected either in the space between the deepest geophysical coverage and the tunnel or laterally in the space between the positioning of the profile and the projection of the western tunnel to the surface (roughly 10 meters apart).

As mentioned before, resolution increases when more clusters are used in the classification of the resistivity and velocity values. When this number becomes seven or eight, the broad middle zone in profile P1_3 seems to be split in two separate zones: one broader to the left and a thinner one to the right. This is an interpretation that is consistent for both results, but again, the internal NGU one seems to generate this differentiation even when five clusters are used. Regardless of these changes concerning the middle area, both results detect a third zone at the beginning of the profile, which seems to be tilting backwards towards a poor bedrock zone in the eastern tunnel. However, this interpretation is dubious since it is found at the edge of the profile where coverage is very shallow and the distance to the tunnel over 40 meters. Finally, six or seven clusters appear to lead to the most reliable results.

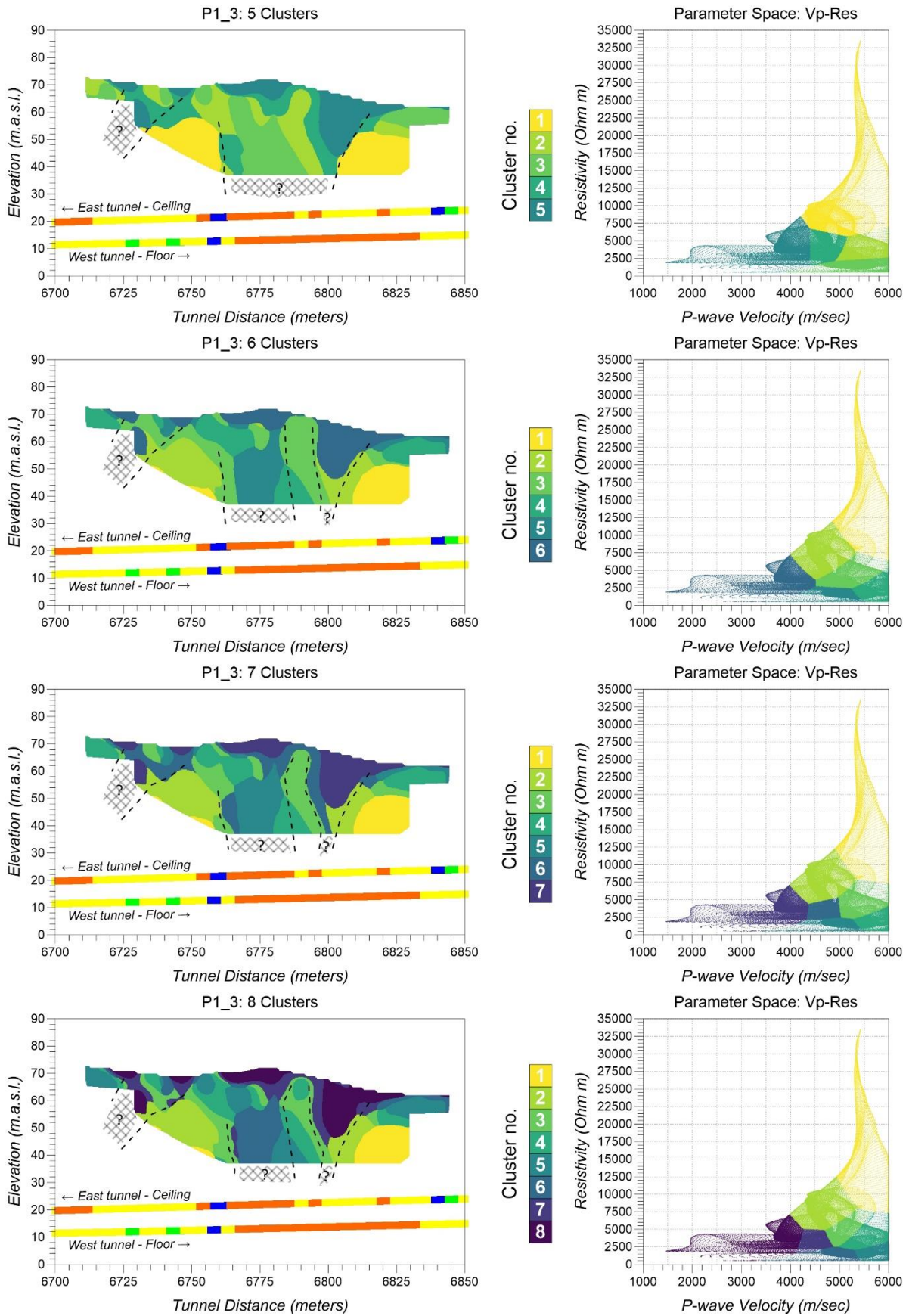


Figure 7: FCM cluster analysis results for Profile P1_3 using five, six, seven and eight clusters (left, top to bottom) and respective parameter space plots (right, top to bottom). Conducted by Dr B. Benjumea.

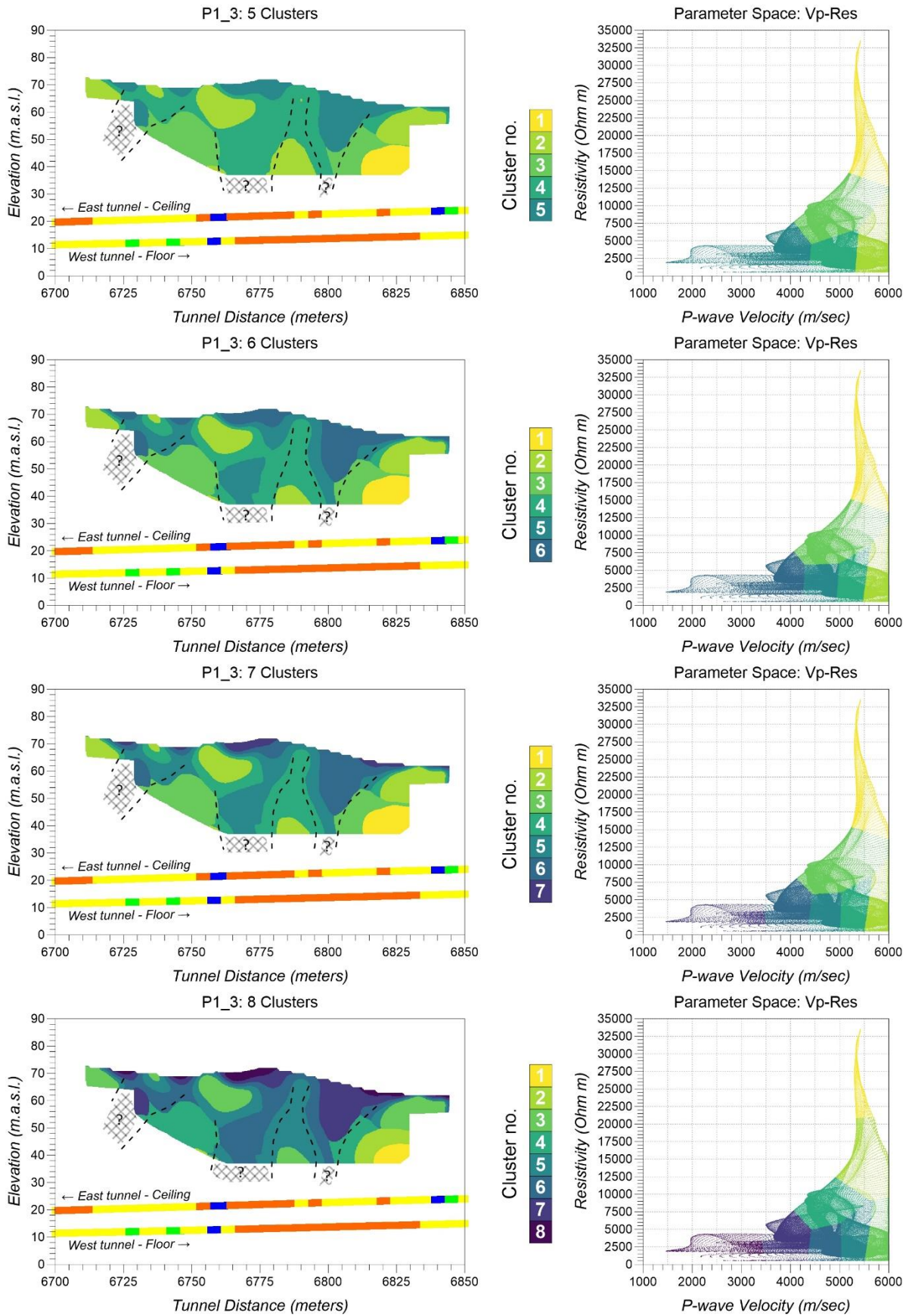


Figure 8: FCM cluster analysis results for Profile P1_3 using five, six, seven and eight clusters (left, top to bottom) and respective parameter space plots (right, top to bottom). Conducted by NGU researcher Ying Wang.

5.4 Profile P1_4-5

Profile P1_4-5 is the first profile in this study whose coverage is deep enough to include the tunnelling and therefore generate interpretations directly comparable to the bedrock quality estimations. The clustering results obtained by both implementations are shown in **figures 9** and **10** respectively, where it is clear to see that the tunnel is located well within the geophysical coverage.

Discrepancies between the geological observations inside the two tunnels seen in the previous profiles is present here too, demonstrating an image of wide sections of poor bedrock quality interchanging with short intervals of good bedrock quality. This is valid in both eastern and western tunnel however, the distribution of these areas is again dissimilar. Nonetheless, observations in both tunnels agree that the middle section of profile P1_4-5 is characterized by worse bedrock conditions whereas better quality is found at the edges.

Like in previous cases, FCM clustering applied on profile P1_4-5 delivers similar results regardless of implementation or number of clusters utilized. Generally, both versions illustrate two wide zones occupying the middle part of the profile that could potentially signify poor bedrock quality, interrupted by an almost vertical feature of improved rock integrity. Even though such a division in bedrock quality is observed in both tunnels, the positioning of these dark green/purple clusters is not matching the evaluated weak zones. Our interpretations show that the first possible weak zone is generally matching what is found in the tunnels but the second one has a significant offset to the right, having its entire second half located at an area of fair to even good bedrock quality. For this cluster distribution to match the geology in the tunnels, the tunnel estimations must be shifted accordingly to the arrows shown in **figures 9** and **10** derived from the superficial geometry of mapped fracture zones. Still, even if this shift is valid, it cannot fully satisfy the allocation of poor bedrock quality in both tunnels. In this sense, we may assume that interpretations on possible weak zones stemming from cluster analysis are closer to the conditions in the western tunnel than in the eastern one.

Small changes in the spatial distribution of clusters have a more pronounced effect in the resulting profiles and this is noticeable our results. First and foremost, the results obtained by the external implementation appear to have more striking chromatic contrasts, especially when more clusters are used. In the same sense, results with the internal NGU implementation have a more balanced transition between colours. For example, the good quality bedrock interpreted between the two possible weak zones, is coloured more lightly on the external results, leading to a different interpretation than the internal NGU results. On the other hand, the profile edges are almost equally lightly coloured and therefore illustrate typically good bedrock quality for both versions of results. Finally, seven clusters appear to be working best for both clustering operations.

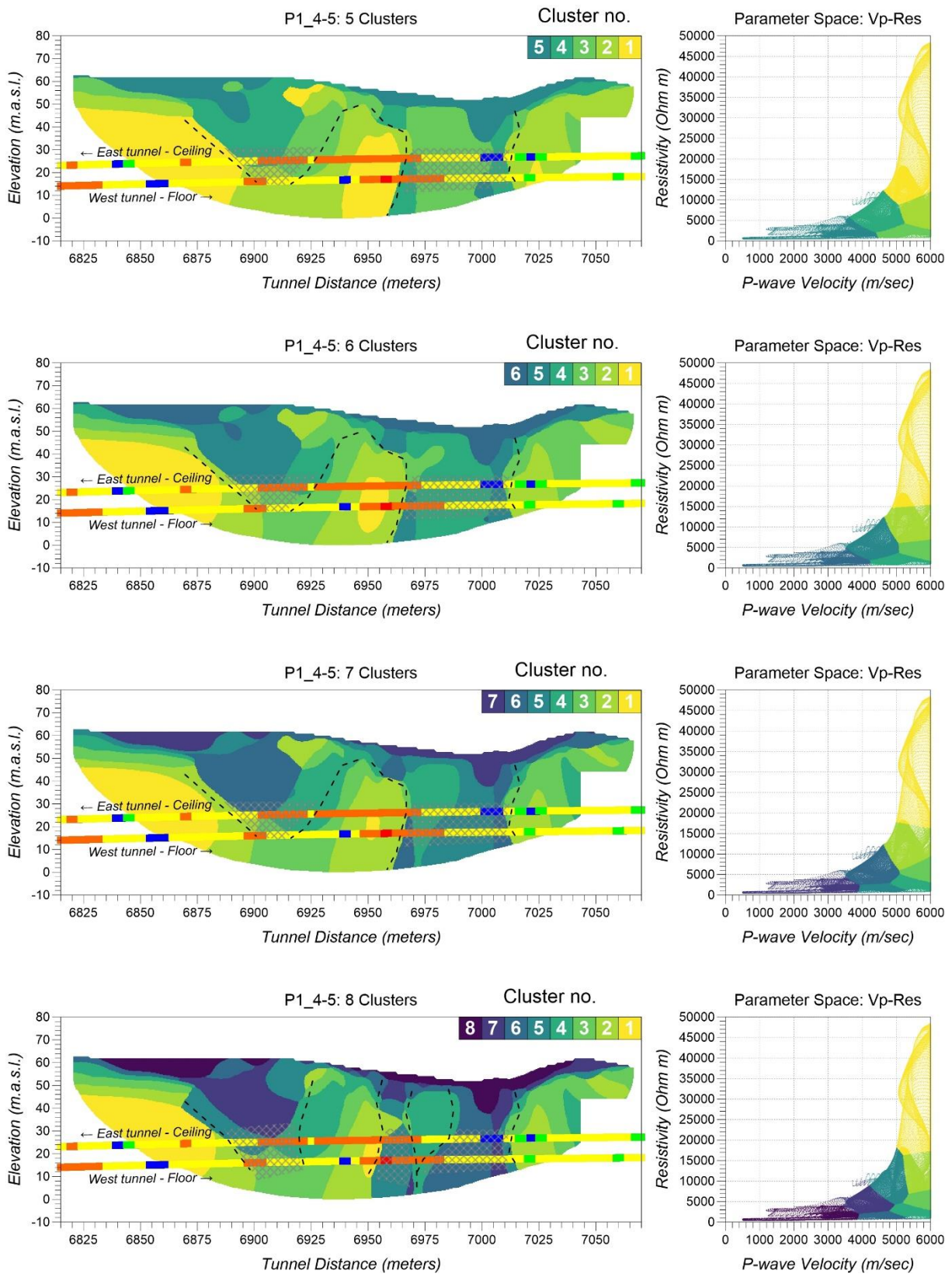


Figure 9: FCM cluster analysis results for Profile P1_4-5 using five, six, seven and eight clusters (left, top to bottom) and respective parameter space plots (right, top to bottom). Conducted by Dr B. Benjumea.

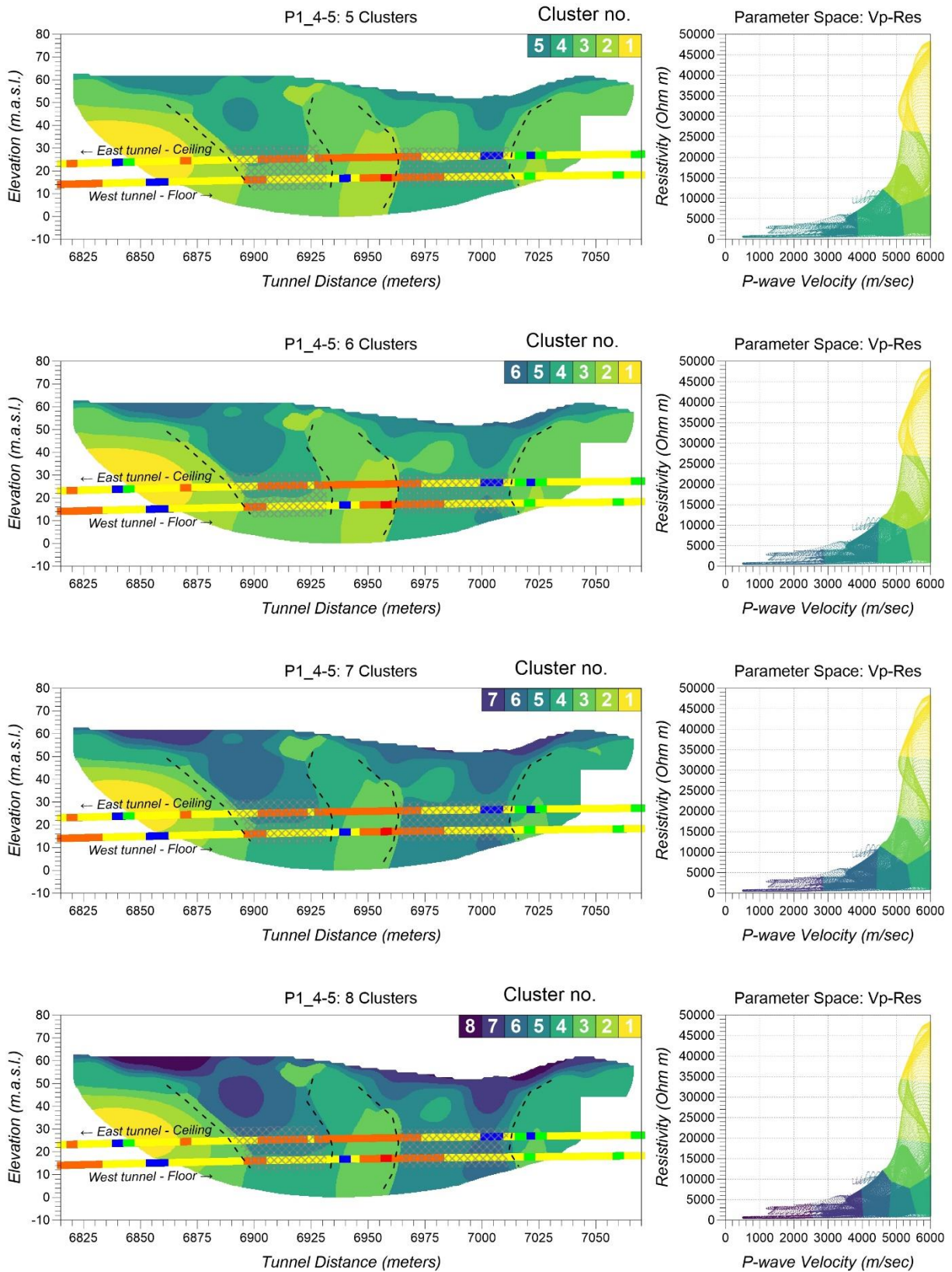


Figure 10: FCM cluster analysis results for Profile P1_4-5 using five, six, seven and eight clusters (left, top to bottom) and respective parameter space plots (right, top to bottom). Conducted by NGU researcher Ying Wang.

5.5 Profile P1_6-7

Like in the previous section, profile P1_6-7 has achieved a coverage deep enough to overlap the level of the two tunnels. **Figure 11** displays the results of applying FCM clustering to this profile with the external implementation, while **figure 12** shows the application results for the internal NGU one. Profile P1_6-7 is positioned over bedrock that is largely unfractured. Observations in the two tunnels indicate fair to good quality bedrock over most of the traverse, with only a few short segments of poor-quality bedrock found in the middle and near the end of the profile. It should also be noted that for this profile, the structural regime mapped on the surface is shifted from SW-NE to NW-SE (**figure 1**). This means that for fractures intersecting the tunnels at that orientation, the eastern tunnel observations should be shifted forward and the western ones backward in order to spatially fit profile P1_6-7 which is positioned between them.

Implementing FCM cluster analysis on profile P1_6-7 returns results that mirror the good bedrock conditions along this line. All outcomes are imaged in mainly light colors (light green/yellow) which in our interpretation scheme indicate good bedrock quality. Most dark colored clusters are concentrated on the surface and possibly represent overburden sediments and not possible fractures. However, on the results where more clusters were employed, a few vertical structures start to manifest in the profile that could be associated with the thin poor bedrock segments found inside the tunnels. The main feature in this context is a mildly north-inclining dark colored zone on the second half of the profile that is relatively wider than the fracture zone observed in the tunnel. This zone is consistently present in all results, regardless of algorithm used or number of clusters employed. It is also always imaged having the same width that is as mentioned not proportional to the small width of the weak zone found in the tunnel. Nevertheless, since this observation is made near the end of the profile, this part of the tunnel is located outside the geophysical coverage and therefore this interpretation's continuation in depth can only be assumed.

Apart from the above-described main feature, with increased number of clusters and therefore resolution, more possibilities for interpreting possible weak zones arise that could be linked to the remaining poor bedrock localities along profile P1_6-7. In this regard, another vertical structure can be interpreted near the profile's northern end in all internal NGU results but only when eight clusters are utilized with the external one. This zone appears to be either vertical or mildly inclining southwards, towards the other poor bedrock localities, potentially becoming a unified structure in depth marked in both tunnels. As for the very narrow zone evaluated in the eastern tunnel and lies exactly in the middle of profile P1_6-7, only the application of the internal NGU implementation can generate a cluster which matches its position, for at least six clusters or more. The external clustering and the use of five clusters for the internal NGU one fail to detect this feature. Hence six or seven clusters are preferable for this case too, since five is too few and eight seems to create some unnatural color transitions that look like artificial effects.

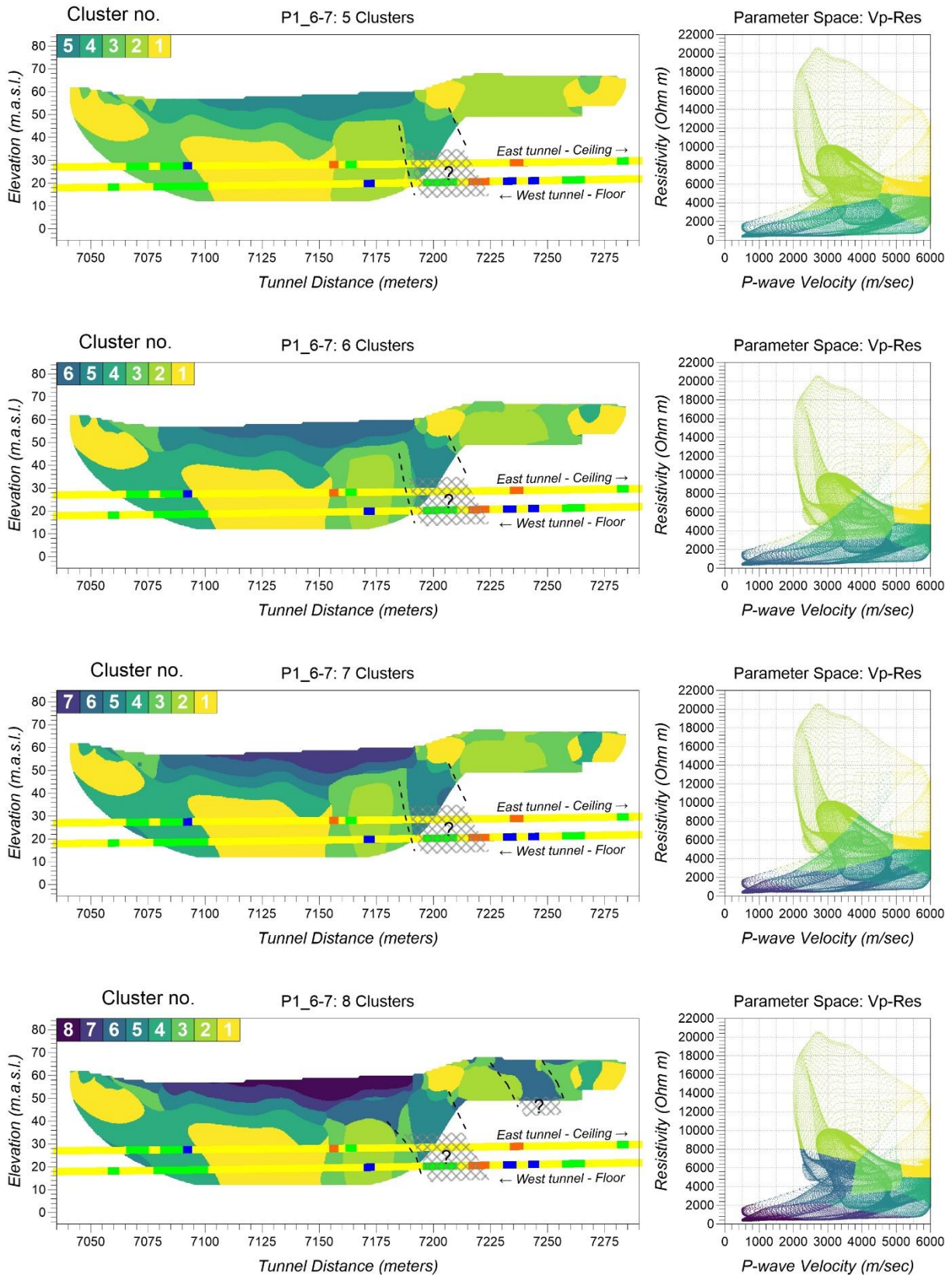


Figure 11: FCM cluster analysis results for Profile P1_6-7 using five, six, seven and eight clusters (left, top to bottom) and respective parameter space plots (right, top to bottom). Conducted by Dr B. Benjumea.

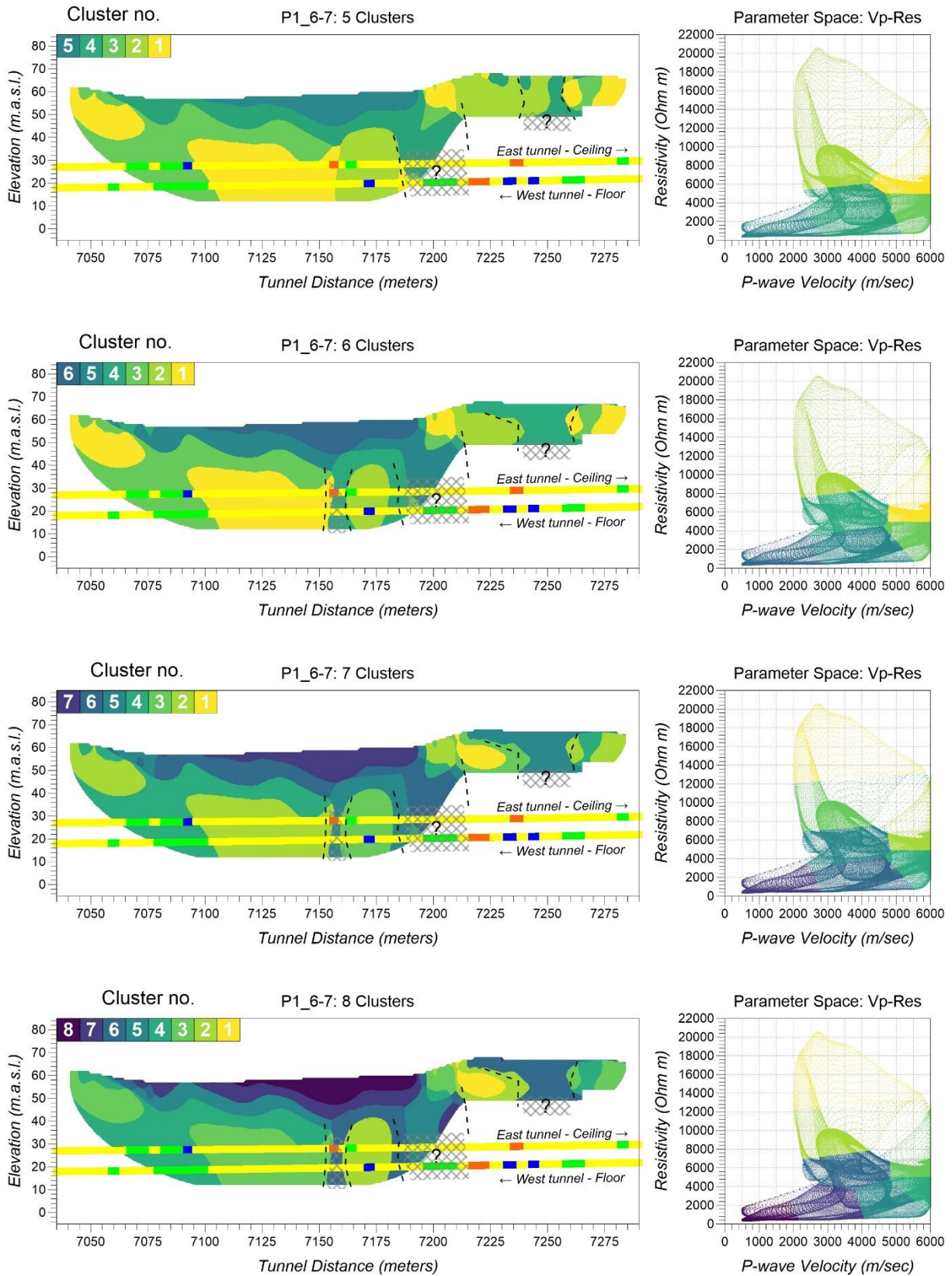


Figure 12: FCM cluster analysis results for Profile P1_6-7 using five, six, seven and eight clusters (left, top to bottom) and respective parameter space plots (right, top to bottom). Conducted by NGU researcher Ying Wang.

5.6 Profile P1_8

With profile P1_8 the condition where the geophysical coverage is not deep enough to include the tunnelling becomes valid again. However, as seen in the clustering results shown in **figures 13** and **14**, the deepest part of the profile's coverage is at least deep enough to be "touching" the ceiling of the tunnel. Therefore, interpretations are only required to be extrapolated over a few meters downwards to actually match the tunnel observations. On the subject of these observations, good bedrock quality is depicted for the majority of the length of the profile, except for the last part where two poor bedrock localities were marked near the end of the profile and mainly inside the eastern tunnel. The fractural regime on the surface is still following the NW-SE direction (**figure 1**) therefore, for the observations in the tunnels to become comparable to the clustering interpretations, a forward shift must be applied for the eastern tunnel and a backward for the western one.

Applying FCM cluster analysis on profile P1_8 has returned a highly consistent cluster distribution regardless of implementation and cluster number employed. All resulting profiles are dominated by light colours (light green/yellow) that indicate good overall bedrock conditions in full agreement with the geological observations in the tunnels. Moreover, increased number of clusters induces small variations in how classifications are arranged in space, locally matching interchanges between fair and good bedrock quality on the first two thirds of profile P1_8. Altogether, bedrock appears to be mainly unfractured beneath 10 meters of overburden materials throughout the bulk of the profile.

Nonetheless, structures characterized by darker colours that could be linked to potential weak zones are found on both edges of profile P1_8. These two zones appear to be tilting outwards, with the first interpreted weak zone to be inclined at a more acute angle than the one at the end of the profile. As seen in all results presented in **figures 13** and **14**, the extrapolation of this first zone is aimed towards a point along the tunnels which is outside the profile's plotted area. Still, it could be potentially associated with weak zones found near the end of the previous profile (P1_6-7, **figures 11** and **12**). The interpreted zone at the end of the profile on the other hand, is more sub-vertical and if we assume the proposed spatial shift of the eastern tunnel's observations, it could match the poor bedrock quality locality marked in that tunnel quite accurately.

On the contrary, the thin weak zone locality found in the second half of the western tunnel, can only be associated with a lateral variation materialized within the light-coloured clusters dominating this area in most clustering results. However, no weak zone can be interpreted at this point on any of our clustering results according to the interpretation scheme that we have adopted in this study. Finally, the external clustering result seems to be more prone to artificial effects especially when higher cluster numbers are used. Again, seven clusters appear to generate the desired resolution for interpreting vertical structures in our data.

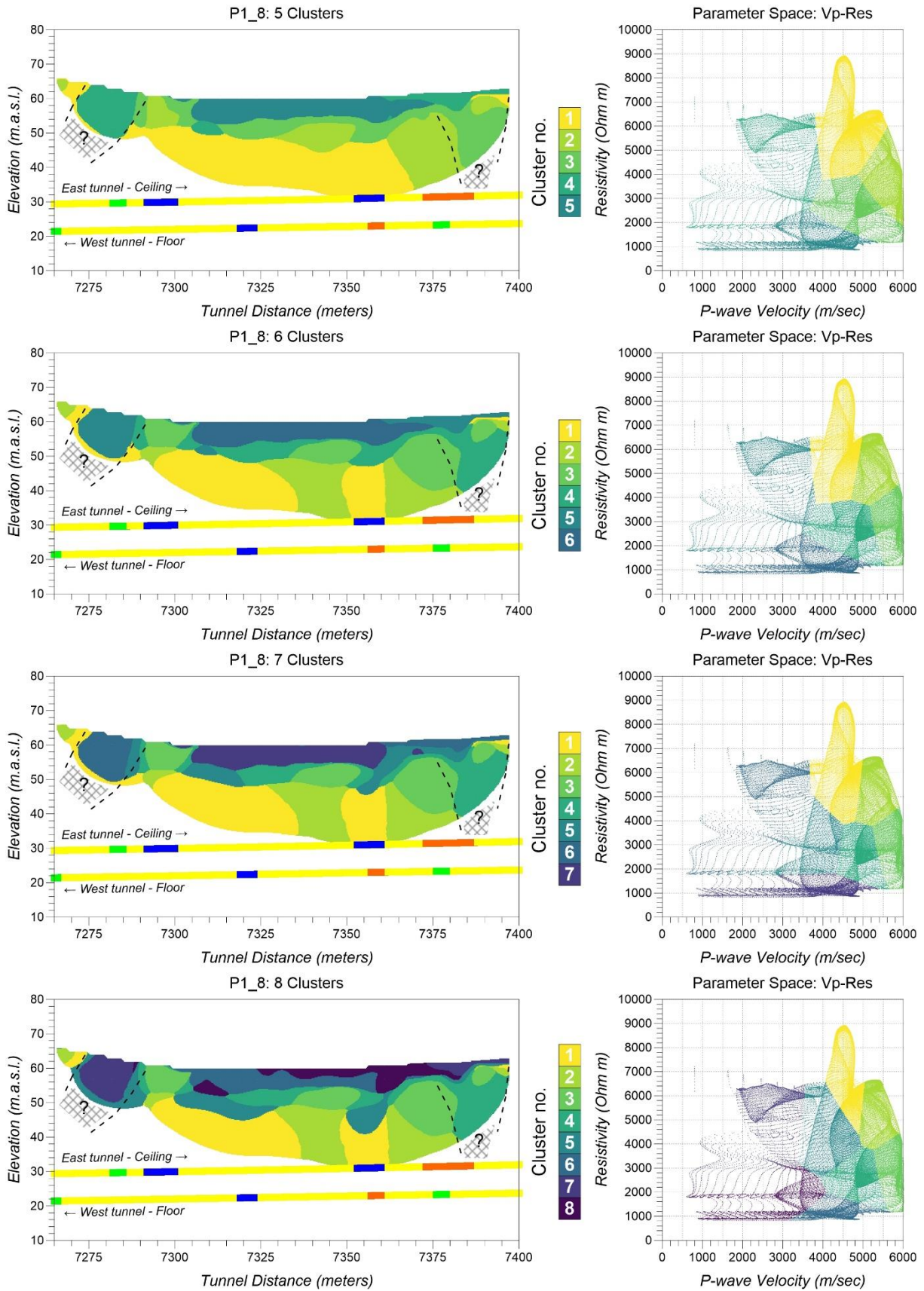


Figure 13: FCM cluster analysis results for Profile P1_8 using five, six, seven and eight clusters (left, top to bottom) and respective parameter space plots (right, top to bottom). Conducted by Dr B. Benjumea.

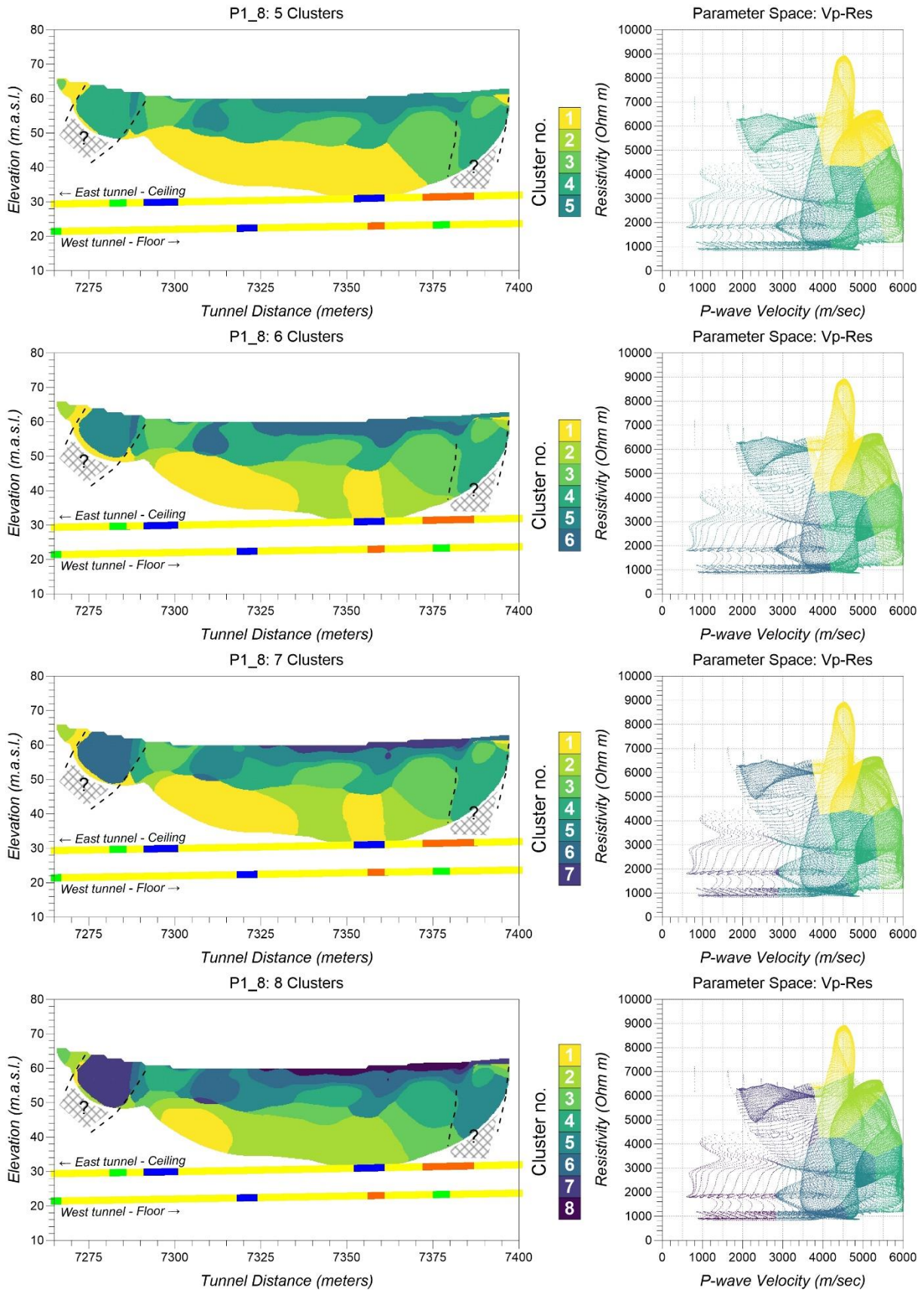


Figure 14: FCM cluster analysis results for Profile P1_8 using five, six, seven and eight clusters (left, top to bottom) and respective parameter space plots (right, top to bottom). Conducted by NGU researcher Ying Wang.

5.7 Profile P1_9

Figures 15 and **16** present the clustering results for profile P1_9 using the external and internal NGU implementation respectively. The deepest coverage of profile P1_9 is again only “touching” the ceiling of the tunnel, but this time at a much larger extent than profile P1_8. This means that interpretations made on these data are positioned very close to the actual observations in the tunnels and therefore quite reliable, especially for the middle part of the profile. For P1_9, observations at the tunnel level appear to be quite inconsistent between the two routes, with the eastern tunnel being evaluated as dominated by consecutive zones of poor bedrock quality, while the western one shows bedrock of much better quality, especially when referring to its second half. When it comes to the directions at which surface fractures cross the tunnel route, mapping indicates a general SW-NE direction. This means that observations must be repositioned in regard to the clustering results with an offset of a few meters forward for the eastern tunnel and backwards for the western one.

At first glance, clustering results appear to be in much better agreement with the geological observations conducted in the eastern tunnel, since all profiles shown in **figures 15** and **16** are dominated by respective clusters of darker colours based on the colour scale utilized. As we have seen before, higher cluster numbers generate higher resolution and the matching between dark-coloured clusters and actual weak zones in the eastern tunnel is relatively good. At the same time, every result obtained regardless of implementation or number of clusters, generates an area at the second half of the profile, which is characterized by mainly yellow colours that are indicative of good quality bedrock. This is in very good agreement with the geological estimations performed in the second part of the western tunnel.

Generally, profile P1_9 positioned between the projection of the two tunnels at the surface and combined with the complex fractural regime in the region, presents a very good example of the strong bias involved in this study. Depending on what is mapped in depth, parts of its clustering results are representative of observations made in both tunnels, but at the same time, no perfect match with either tunnel is achieved. This highlights the need for matching positioning between geophysics and tunnelling, especially when cluster analysis is to be applied. With that being said, clustering appears to generate classes in our data that are not far from reality and produce joint interpretations between resistivity and P-wave velocity that exploit the advantages of both methods.

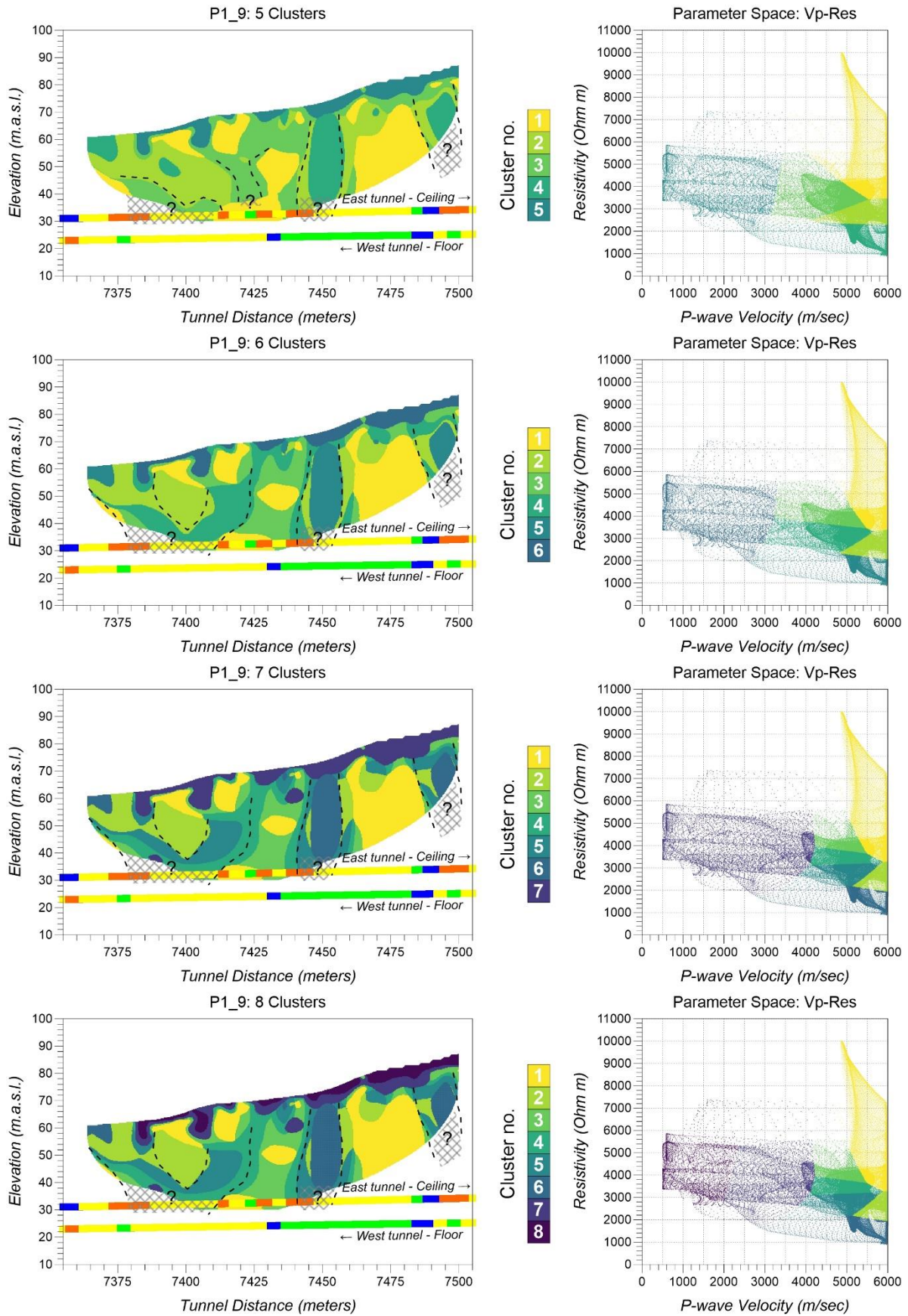


Figure 15: FCM cluster analysis results for Profile P1_9 using five, six, seven and eight clusters (left, top to bottom) and respective parameter space plots (right, top to bottom). Conducted by Dr B. Benjumea.

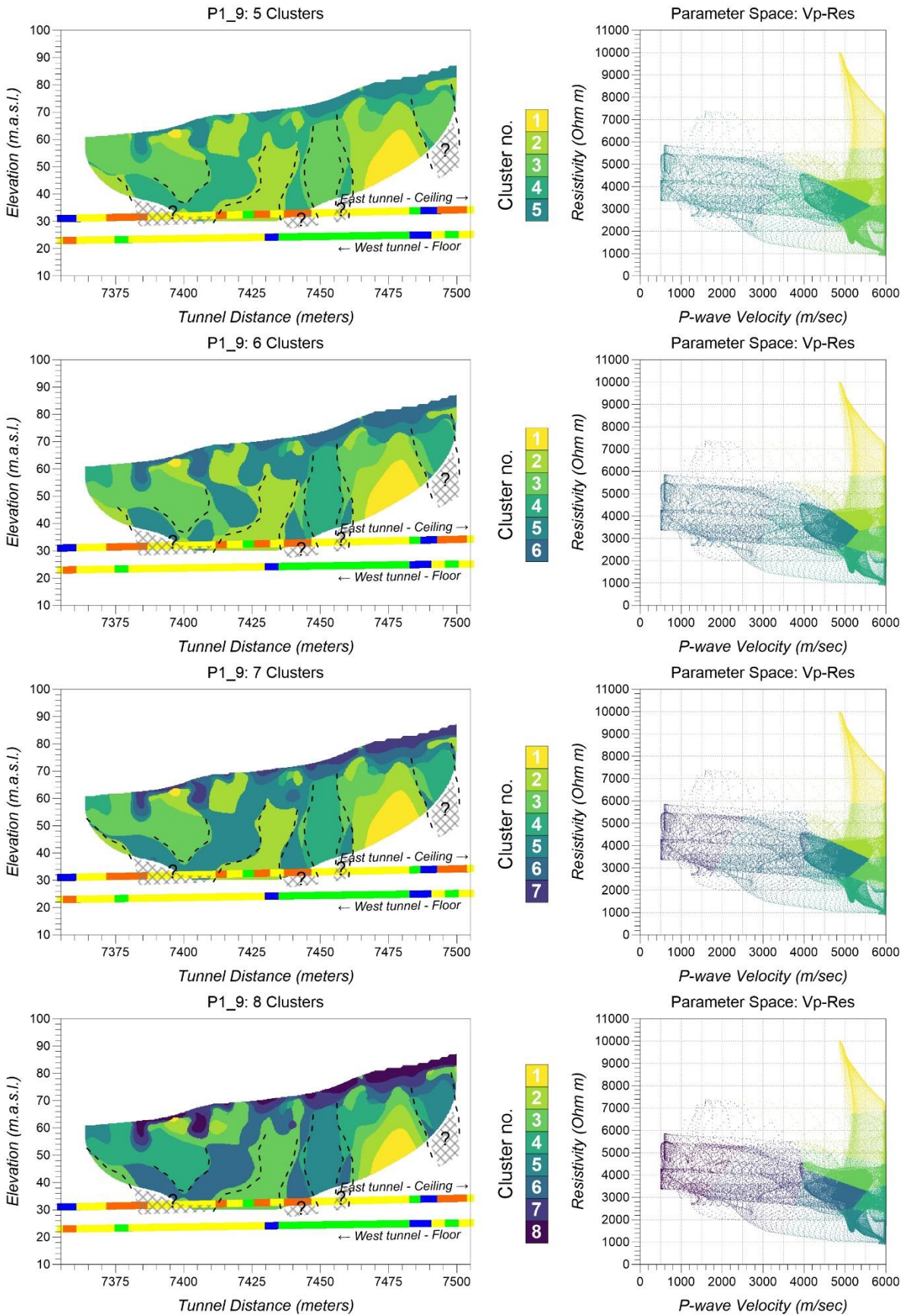


Figure 16: FCM cluster analysis results for Profile P1_9 using five, six, seven and eight clusters (left, top to bottom) and respective parameter space plots (right, top to bottom). Conducted by NGU researcher Ying Wang.

5.8 Profile P1_9.5

Profile P1_9.5 is a shorter supplementary profile planned to investigate a superficial fracture zone that was mapped a few meters after the end of profile P1_9 (**figure 1**). Due to its limited length and uphill positioning, the profile's coverage is stopping at 20-30 above the tunnel and therefore interpretations have to be extrapolated downward to reach the tunnel level as in previous cases. Concerning the geological observations in depth and since a big part of profile P1_9 is also investigated in profile P1_9.5, there is a striking mismatch between bedrock quality evaluated in each tunnel. The eastern tunnel is characterized by much worse bedrock conditions when compared to the western one, within which bedrock quality observed was described as at least fair. In this sense, the main focus will be to produce interpretations on the FCM cluster analysis results shown in **figures 17** and **18** that will potentially match the conditions mapped inside the eastern tunnel.

For the case of profile P1_9.5, both versions of implementation utilized generate results that illustrate three vertical or sub-vertical structures that are coloured in different hues of dark green/purple colours, according to the number of clusters selected. Applying our interpretation scheme on the external algorithm results, possible weak zones can be assigned to the 2nd and 3rd vertical structures (**figure 17**). For this interpretation to be valid, the eastern tunnel observations must again be shifted forward, which is in good agreement with the SW-NE orientation of the superficial fractures. On the other hand, the same interpretation scheme applied on the FCM cluster analysis results using the internal NGU solution, yields that it is more probable for the 1st and 3rd vertical structure to be weak zones. Moreover, these interpretations do not require the shifting of the quality estimations conducted in the eastern tunnel in order to achieve a good match with the two poor bedrock quality zones found in the tunnel. Hence, the two implementations utilized do not produce different qualitative results since the clustering layout is roughly similar for both sets of results, but instead different quantitative images where different colour distributions lead to different interpretations.

Nevertheless, both clustering attempts agree on the significance of the 3rd vertical structure in profile P1_9.5 and image the gradual decrease in bedrock quality pretty well, with yellow colours turning into dark green as good quality bedrock degrades to a weak zone as we move northwards. This is in fact a qualitative interpretation that could also satisfy what was mapped inside the western tunnel too, since bedrock evaluations delineate good bedrock quality flanked by relatively worse rock conditions on both sides. Lastly, the selection of seven clusters is verified once more as the best choice for this dataset, regardless of implementation.

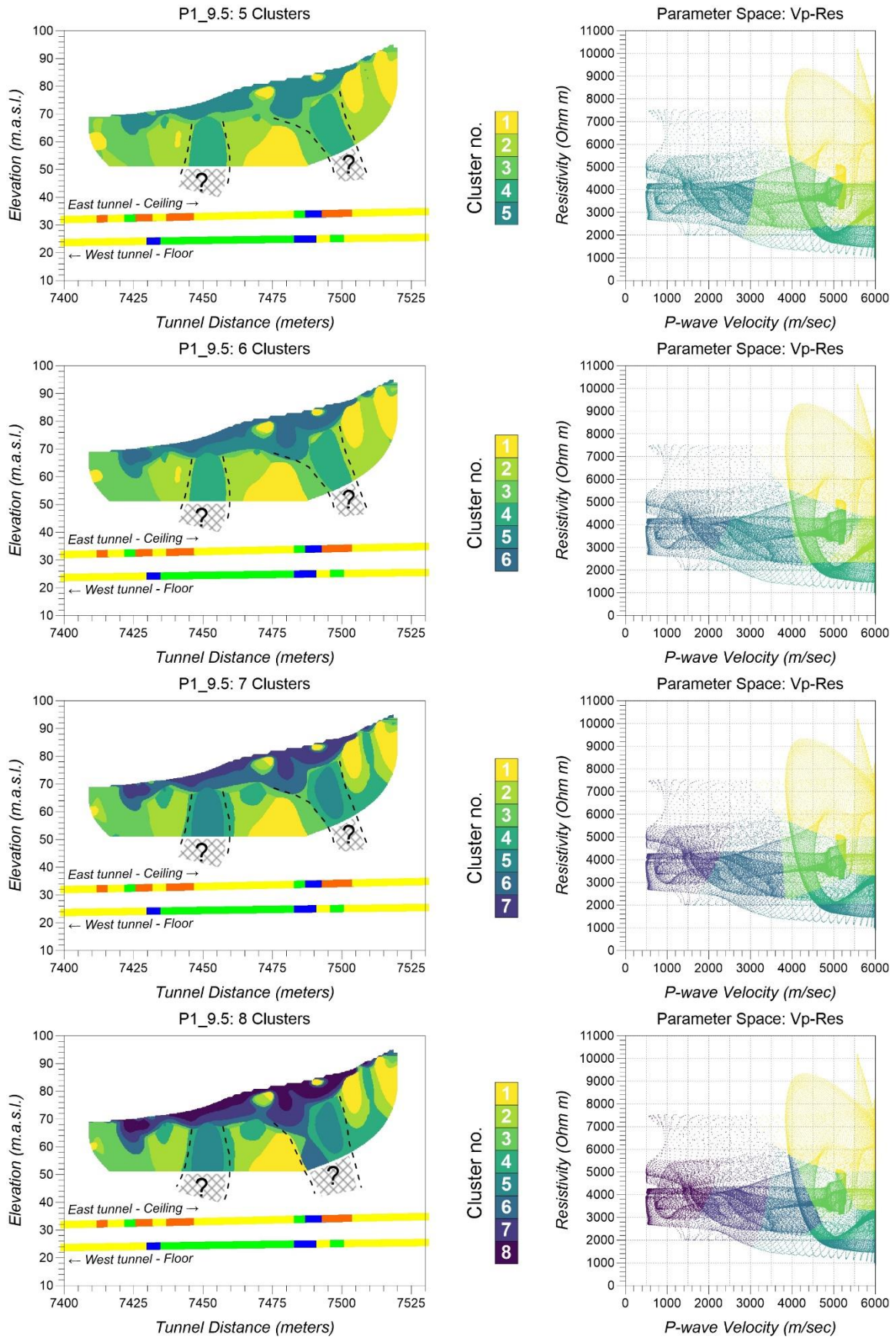


Figure 17: FCM cluster analysis results for Profile P1_9.5 using five, six, seven and eight clusters (left, top to bottom) and respective parameter space plots (right, top to bottom). Conducted by Dr B. Benjumea.

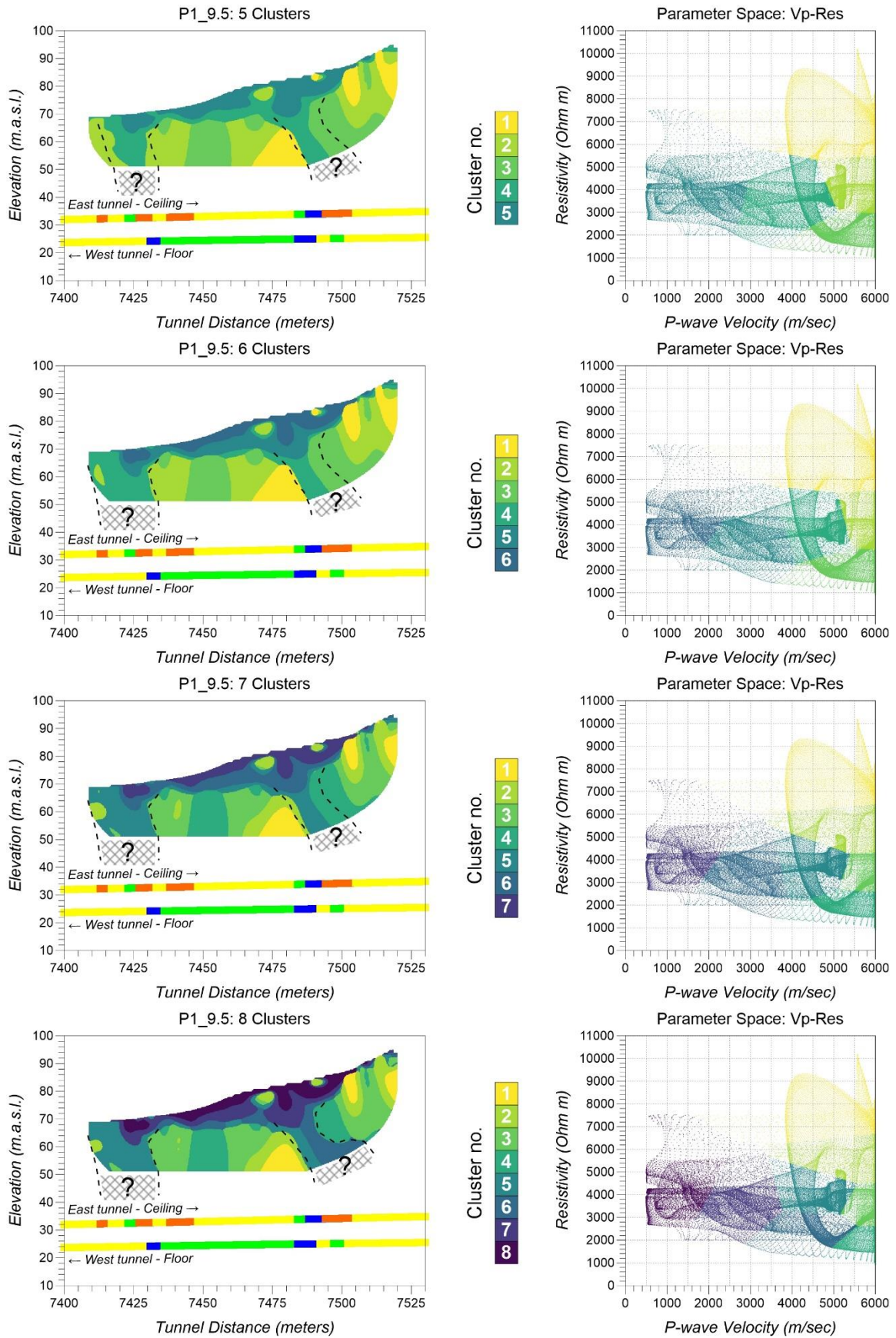


Figure 18: FCM cluster analysis results for Profile P1_9.5 using five, six, seven and eight clusters (left, top to bottom) and respective parameter space plots (right, top to bottom). Conducted by NGU researcher Ying Wang.

5.9 Profile P3

Profile P3 is a line positioned north of the area covered by line P1 consisted of the previous eight sub-profiles in order to investigate a locality where a significant superficial SW-NE trending weak zone was mapped crossing the tunnel (**figure 2**). As opposed to all other cases examined in this report, profile P3 is located exactly over the eastern tunnel, following its route on the surface. Therefore, interpretations performed on the clustering results for this profile are the most directly comparable ones to the observations in the tunnel in this study. However, inaccuracies related to the positioning of the ERT line and the tunnelling itself are still a source for discrepancies.

Figures 19 and **20** present the FCM clustering results for profile P3 using external and internal NGU implementations respectively, together with bedrock quality estimations along the eastern tunnel. The profile's coverage is stopping a few meters above the ceiling of the tunnel, but the distance is no greater than 5-10 meters. Bedrock conditions appear to be good except for a very prominent very poor bedrock quality zone found at the beginning of the profile. This tunnel zone is misplaced in relation to the superficial fracture mapped, since **figure 2** shows that it is crossing the profile near its end and not at its beginning.

Results display again a difference in cluster distribution which is translated into more sharp colour transitions when the external implementation is used (**figure 19**) and a smoother assortment for the internal NGU one (**figure 20**). In this sense, both versions detect a series of vertical structures but the external one is more prone to artificial effects, especially as the cluster number increases. Interpretation of possible weak zones on the results of **figure 19** becomes challenging with each different cluster number and therefore no zones can be consistently interpreted. However, five and six clusters reveal two possible weak zone structures, one roughly matching the very poor bedrock locality at the tunnel and the other matching the fracture zone mapped on the surface. Interestingly enough, no poor bedrock has been observed at that segment of the tunnel, even though the cluster assigned to this area signifies "worse" conditions than the one describing the first zone in profile P3.

The use of the internal NGU FCM implementation shown in **figure 20** returns more consistent results regardless of clusters employed, but the interpreted setting is the same as before. Two zones matching tunnel and superficial fracture observations respectively, with the surface feature not being reflected at the tunnel level. Nonetheless, clustering results with this implementation offer a possible explanation due to the fact that the area before the second zone is also characterized by dark green colours but truncated upwards. Considering also that the original ERT and Refraction Seismic processing was "guided" towards revealing vertical structures – an effect definitely carried over into our cluster analysis results – we have possibly transformed a dipping zone which is shown in the form of a red dotted line in both **figure 19** and **20** into fragmented vertical structures. Therefore, the continuation of the second vertical structure in depth is possibly an artificial effect of steering pre-processing. Traces of such an inclined structure exist in all clustering results once they have been identified using the internal NGU solution.

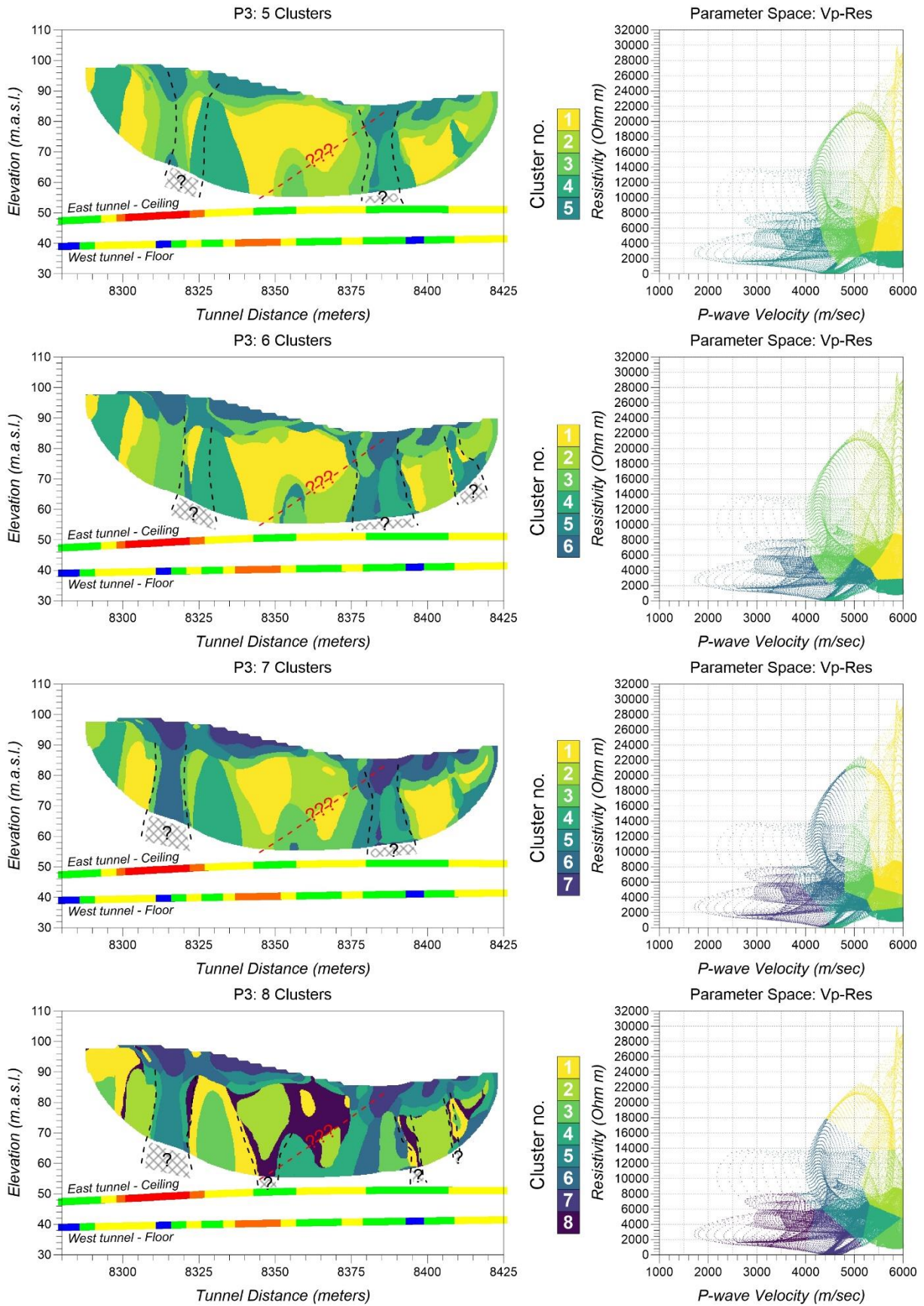


Figure 19: FCM cluster analysis results for Profile P3 using five, six, seven and eight clusters (left, top to bottom) and respective parameter space plots (right, top to bottom). Conducted by Dr B. Benjumea.

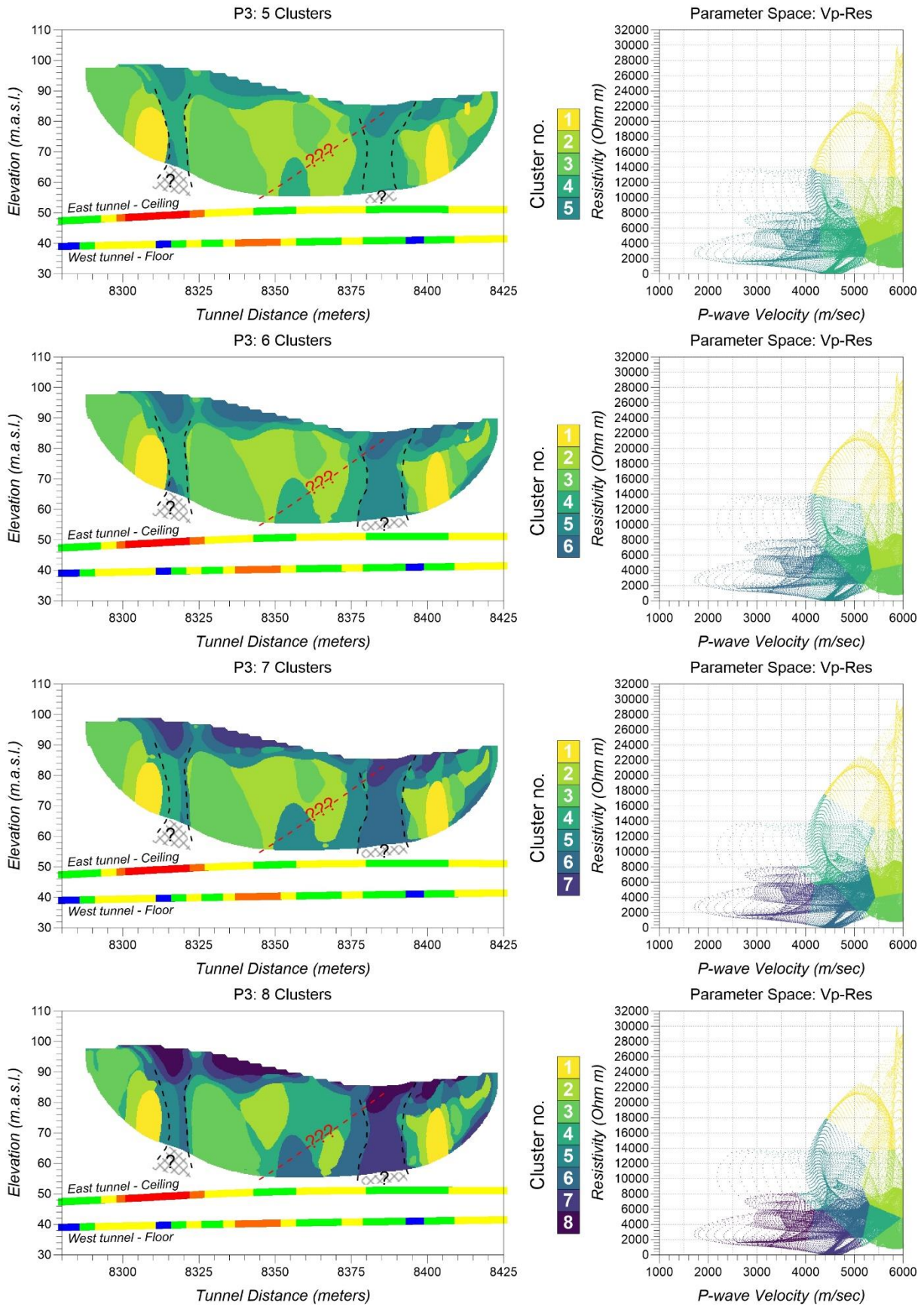


Figure 20: FCM cluster analysis results for Profile P3 using five, six, seven and eight clusters (left, top to bottom) and respective parameter space plots (right, top to bottom). Conducted by NGU researcher Ying Wang.

5.10 Profile P6

As seen in **figure 2**, the last profile examined in this study namely profile P6 was measured a few hundred meters south of profile P3 but is essentially serving the same purpose i.e., to investigate the underground continuation of a fracture mapped at the surface. It was again collected between the projection of the two tunnels to the surface and therefore observations in the tunnels must be shifted in accordance with the direction of the superficial lineaments intersecting them to be comparable to the interpretations done on the cluster analysis results.

After applying FCM cluster analysis on the geophysics measured along line P6, we have obtained the results shown in **figures 21** and **22**. From these figures it is discernible that interpretations must be extrapolated over a long distance in depth since the deepest coverage achieved is more than 60 meters away from the tunnel level. In this sense, the main focus here is at the beginning of the profile where the superficial weak zone is intersecting it and how clustering correlates with observations made at the tunnels. Regarding those, both tunnels begin with poor bedrock segments but then quality becomes gradually better as we move northwards. Again, direction for shifting in positioning of these observations in relation to the SW-NE direction of the superficial weak zone, is marked in all figures.

Results for profile P6 indicate that both FCM implementations return a very specific structure for how clusters are distributed. All profiles presented in **figures 21** and **22** are characterized by a lateral shift in colour that mirrors the improvement in bedrock quality as we move northwards. The first one third of profile P6 is characterized by dark coloured clusters which is gradually shifting to brighter ones farther along the line. This zone is in excellent agreement with observations made in the western tunnel, especially if the forward shift is assumed. Concerning the eastern tunnel, the match is not equally good but the area which is not covered by geophysics is too great to make any assessment concerning the geometry of such a feature.

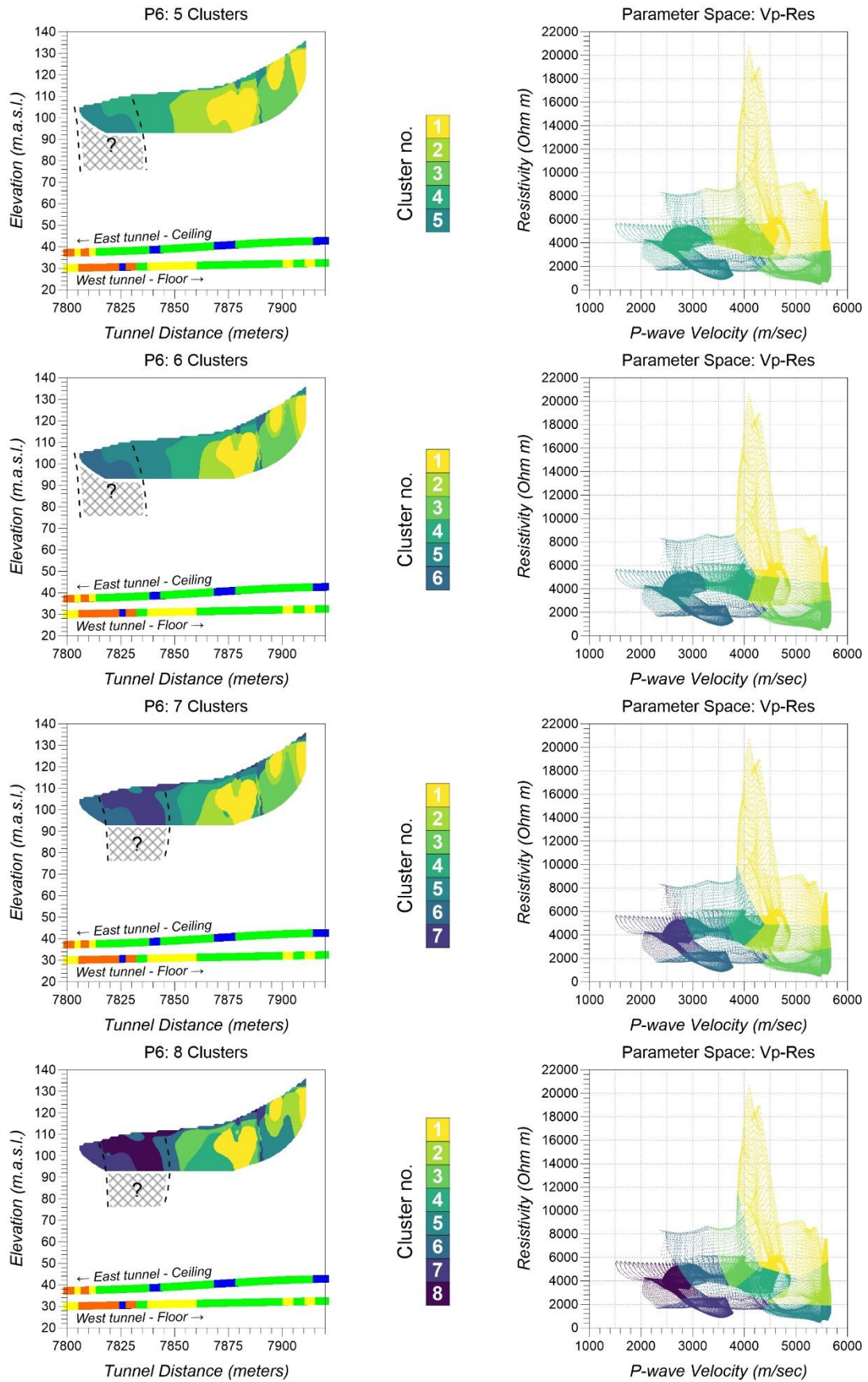


Figure 21: FCM cluster analysis results for Profile P6 using five, six, seven and eight clusters (left, top to bottom) and respective parameter space plots (right, top to bottom). Conducted by Dr B. Benjumea.

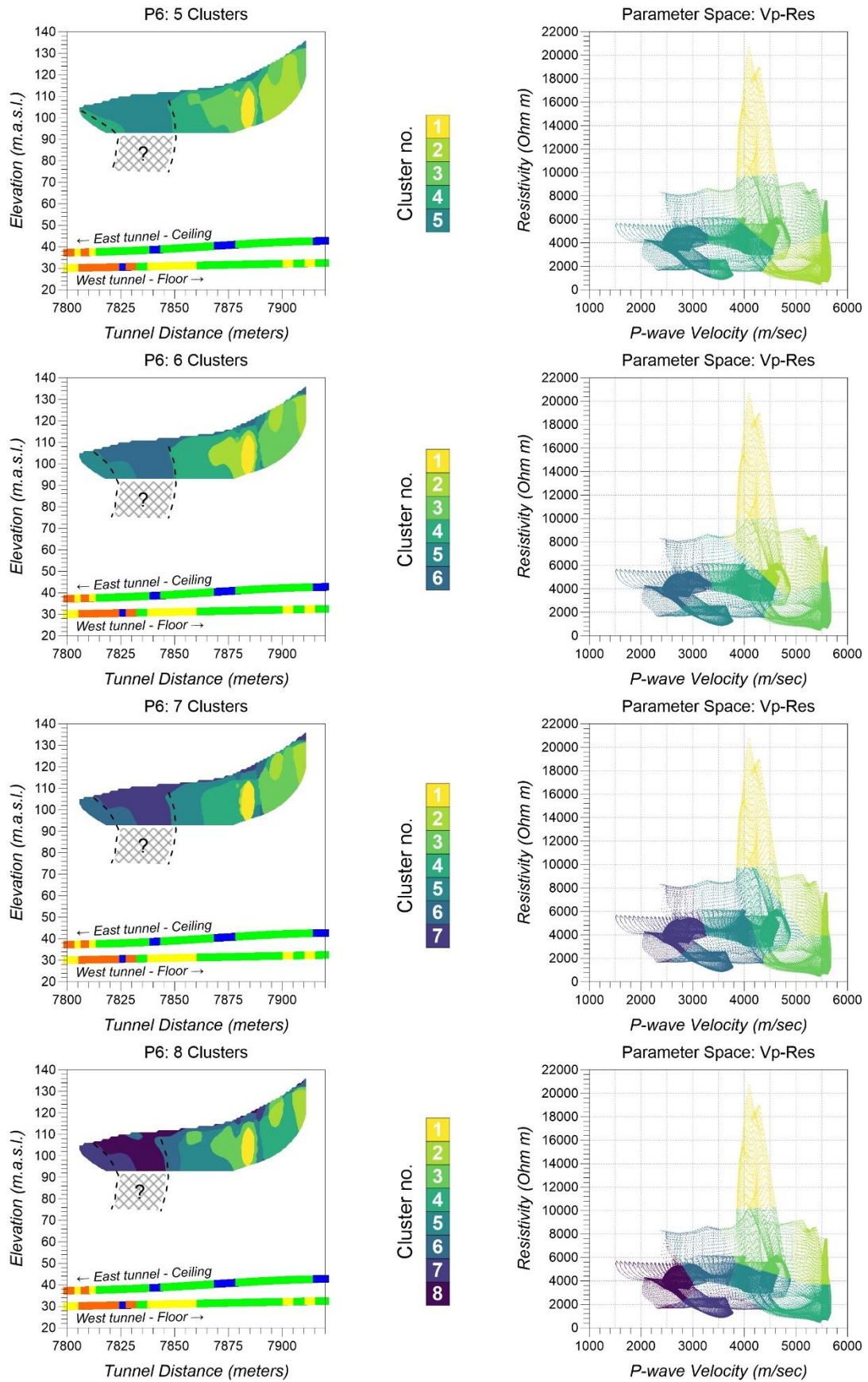


Figure 22: FCM cluster analysis results for Profile P6 using five, six, seven and eight clusters (left, top to bottom) and respective parameter space plots (right, top to bottom). Conducted by NGU researcher Ying Wang.

6. DISCUSSIONS & CONCLUSIONS

In this study, we have attempted to jointly interpret ERT and Refraction Seismic inversion results by applying cluster analysis which classifies pairs of resistivity and P-wave velocity with the use of two different algorithms. The performance of FCM clustering was evaluated based on the resulting correlation between different clusters (five to eight were examined) and segments inside the tunnel where poor and very poor bedrock was observed after the completion of the road. Even though basic standards such as co-location for profiles were more or less met, the work presented here is subject to improvement for reasons mostly related to poor positioning information and limited experience on the topic of bringing geophysical parameters together on the vertical 2D sense.

Coming up with a cluster colouring pattern that would reflect the transition from better to worse bedrock quality was a very challenging task. We have therefore experienced clusters being formed that had distinct numerical features but little physical meaning such as pairing up low resistivities with high P-wave velocities and vice versa. Our colouring strategy in the end, followed a concentric pattern in the parameter space, using essentially fewer “standard” colours in our effort to make clustering results as physically sound as possible and easily interpretable. In that context, we can state that our colour scale strategy worked well for both versions of FCM implementation results, but our interpretation was still quite intuitive and not entirely driven by the clusters themselves.

The two independent implementations returned clustering results that were very similar in appearance but not identical. The external version yielded sharper colour transitions and as the cluster number was increasing, it was becoming more prone to artificial effects. The internal NGU version generated smoother images and results were more consistent regardless of the number of clusters picked. Nonetheless, both applications showed that five and sometimes six clusters fail to induce the desired resolution to our data in order for vertical structures to become highlighted. Utilizing eight clusters on the other hand caused unnatural cluster distributions in our data, in addition to creating even more challenges in establishing a satisfactory colour scale. For the cases examined in this study, seven clusters appear to be the most balanced choice, even though different data sets may require testing before selecting the ideal number.

Interpretation based on the dark-coloured clusters for possible weak zones and the more light-coloured ones for unfractured bedrock showed a good overall agreement with bedrock quality that was mapped inside the tunnels. However, mismatches were observed that were due to a variety of reasons independent to clustering such as:

- the complexity of the geological setting in the area with fractures intersecting the tunnel route in acute angles,
- problems linked to bad or imperfect positioning (inaccurate ERT positioning, positioning of lines between the projection of the tunnels to the surface, inaccuracies in relation with positioning of geological observations inside the tunnels, etc.),
- significant discrepancies between the geological bedrock quality estimations made in each tunnel showing big changes happening over short distances.

In order to avoid such errors in future surveys, that include measuring of multiple ground geophysics 2D profiles, accurate positioning must be guaranteed for all factors coming into play.

There are also improvements to be made on the pre-processing stages preceding the implementation of cluster analysis. In this study, we have fed both implementations with the true inverted resistivity and P-wave velocity values. However, resistivity is a physical parameter that is usually plotted in the logarithmic domain. Plotting logarithmic resistivity against velocity on the parameter space would result in a more robust distribution and possibly to more meaningful clustering results. In addition, clustering applied on the entire dataset (all inverted values merged in one file) would also lead to more uniform results and help indicate individual differences in each profile compared to the overall regime in the area. Lastly, inversion schemes applied individually on ERT and Refraction Seismic data before their results are fed into the clustering algorithm should also be considered. In this case, “robust” inverted data that inherently suppress inclined features were inherited in cluster analysis, further strengthening the masking of inclined features in favour of vertical structures. In this context, joint inversion for ERT and Refraction Seismic data and then feeding those interconnected results to a clustering algorithm could also be interesting to test in the future.

Admittedly, the power of the internal NGU fuzzy *c*-means algorithm is not fully utilized in this study. We have assigned each data point a cluster number with the highest membership score resulting from the algorithm, while its membership scores to other clusters (the ‘fuzziness’) are not reflected in the final cluster map. The focus here is to highlight spatial heterogeneity of the depth section, while including the fuzziness element contributes more to the interpretation aspect. More specifically, the fuzziness can help delineating overlapping clusters, that is, the ‘grey’ areas. Visualization and analysis of the fuzziness measure are among our immediate action plans as the project proceeds from broad understanding to detailed studies.

7. REFERENCES

- Benjumea, B., Gabàs, A., Macau, A., Ledo, J., Bellmunt, F., Figueras, S. & Piña, J., 2021. Undercover karst imaging using a Fuzzy c-means data clustering approach (Costa Brava, NE Spain), *Engineering Geology*, Volume 293, 106327, ISSN 0013-7952, <https://doi.org/10.1016/j.enggeo.2021.106327>.
- Bezdek, J.C., Ehrlich, R. & Full, W., 1984. FCM: the fuzzy c-means clustering algorithm. *Computers & Geosciences*, 10, 191-203.
- Caliński, T. & Harabasz, J., 1974. A Dendrite Method for Cluster Analysis. *Communications in Statistics-theory and Methods*, 3, 1-27.
- Ganerød, G.V., Dalsegg, E. & Rønning, J.S. 2009: Geologiske og geofysiske undersøkelser for tunnelstrekning Sandeide-Liavatnet, Ringveg Vest, Bergen. NGU Rapport 2009.077, 23 pp.
- Hellman, K., Ronczka, M., Günther, T., Wennermark, M., Rücker, C. & Dahlin, T. 2017. Structurally coupled inversion of ERT and refraction seismic data combined with cluster-based model integration, *Journal of Applied Geophysics*, Volume 143, Pages 169-181, ISSN 0926-9851, <https://doi.org/10.1016/j.jappgeo.2017.06.008>.
- Norge i Bilder, 2022: Bergen Orthophoto, www.norgebilder.no.
- Paasche, H. & Eberle, D., 2011. Automated compilation of pseudo-lithology maps from geophysical data sets: a comparison of Gustafson-Kessel and fuzzy c-means cluster algorithms. *Exploration Geophysics*, 42, 275-285.
- Loke, M.H. 2018: RES2DINV x64 ver. 4.07.11. Geoelectrical Imaging 2D & 3D. Instruction manual. www.geoelectrical.com.
- Novák, V., Perfilieva, I. & Mockor, J., 1999. *Mathematical Principles of Fuzzy Logic*. Kluwer Academic Publishers, Dordrecht, The Netherlands, 320p.
- Rohdewald, S. 2018: Rayfract version 3.35. Seismic Refraction & Borehole Tomography- Subsurface Seismic Velocity Models for Geotechnical Engineering and Exploration. Download from <http://rayfract.com>.
- Rønning, J.S., Tassis, G., Kirkeby, T. & Wåle, M. 2016: Retolkning av geofysiske data og sammenligning med resultater fra tunneldriving, Knappetunnelen ved Ringveg Vest i Bergen. NGU rapport 2016.048 (48s.). http://www.ngu.no/upload/Publikasjoner/Rapporter/2016/2016_048.pdf.
- Rønning, J.S., Tassis, G., Kirkeby, T. & Wåle, M. 2019: Reprosessering og ny samtolkning av geofysiske data med resultater fra tunneldriving, Knappetunnelen ved Ringveg Vest i Bergen. NGU Rapport 2019.014 (57s.). https://www.ngu.no/upload/Publikasjoner/Rapporter/2019/2019_014.pdf.
- Rønning, J.S., Tassis, G., Wisen, R. & Turesson, B. 2020: Tomographic inversion of synthetic refraction seismic data. Quality of inversion using various off-end shots, fracture zones depth, fracture zone velocity, soil thickness and hidden layer thickness. NGU Report 2020.044 (53s.).
- Song, C.Y., Liu, Z.N., Cai, H.P., Wang, Y.J., Li, X.M. & Hu, G.M., 2017: Unsupervised seismic facies analysis with spatial constraints using regularized fuzzy c-means, *Journal of Geophysics and Engineering*, Vol.14-6, 1535–1543.

- Tassis, G., Rønning, J.S. & Rohdewald, S. 2017: Refraction seismic modelling and inversion for the detection of fracture zones in bedrock with the use of Rayfract software. NGU Report 2017.025 (62pp.).
http://www.ngu.no/upload/Publikasjoner/Rapporter/2017/2017_025.pdf.
- Tassis, G., Rohdewald, S. & Rønning J.S. 2018: Tomographic Inversion of Synthetic Data Using Various Starting Models in Rayfract ® software. NGU Report 2018.015 (45pp.).
https://www.ngu.no/upload/Publikasjoner/Rapporter/2018/2018_015.pdf.
- Rousseeuw, Peter J., 1987. Silhouettes: a Graphical Aid to the Interpretation and Validation of Cluster Analysis. Computational and Applied Mathematics, 20, 53–65.
- Thorndike, Robert L., 1953. Who Belongs in the Family? Psychometrika, 18, 267–276.
- Wang, Y., Ksienzyk, A.K., Liu, M. and Brønner, M., 2021. Multi-geophysical data integration using cluster analysis: Assisting geological mapping in Trøndelag, Mid-Norway. Geophysical Journal International, 225(2), 1142-1157. DOI: <https://doi.org/10.1093/gji/ggaa571>.
- Warner, J. et al., 2019. Scikit-Fuzzy version 0.4.2
<https://doi.org/10.5281/zenodo.3541386>.



GEOLOGICAL
SURVEY OF
NORWAY

· NGU ·

Geological Survey of Norway
PO Box 6315, Sluppen
N-7491 Trondheim, Norway

Visitor address
Leiv Eirikssons vei 39
7040 Trondheim

Tel (+ 47) 73 90 40 00
E-mail ngu@ngu.no
Web www.ngu.no/en-gb/